© 2016. Published by The Company of Biologists Ltd | Development (2016) 143, 2907-2919 doi:10.1242/dev.132340

JAK/STAT signalling mediates cell survival in response to tissue stress

Marco La Fortezza, Madlin Schenk, Andrea Cosolo, Addie Kolybaba, Isabelle Grass and Anne-Kathrin Classen*

ABSTRACT

Tissue homeostasis relies on the ability of tissues to respond to stress. Tissue regeneration and tumour models in *Drosophila* have shown that c-Jun amino-terminal kinase (JNK) acts as a prominent stress-response pathway promoting injury-induced apoptosis and compensatory proliferation. A central question remaining unanswered is how both responses are balanced by activation of a single pathway. Signalling through the Janus kinase/Signal transducers and activators of transcription (JAK/STAT) pathway, which is a potential JNK target, is implicated in promoting compensatory proliferation. While we observe JAK/STAT activation in imaginal discs upon damage, our data demonstrate that JAK/STAT and its downstream effector Zfh2 promote the survival of JNK signalling cells. The JNK component *fos* and the pro-apoptotic gene *hid* are regulated in a JAK/STAT-dependent manner. This molecular pathway restrains JNK-induced apoptosis and spatial propagation of JNK signalling, thereby limiting the extent of tissue damage, as well as facilitating systemic and proliferative responses to injury. We find that the pro-survival function of JAK/STAT also drives tumour growth under conditions of chronic stress. Our study defines the function of JAK/STAT in tissue stress and illustrates how crosstalk between conserved signalling pathways establishes an intricate equilibrium between proliferation, apoptosis and survival to restore tissue homeostasis.

KEY WORDS: JAK/STAT, JNK, Cell survival, Compensatory proliferation, Cancer, Injury-induced apoptosis, Eiger, Cell ablation

INTRODUCTION

Tissue homeostasis relies on the ability of tissues to respond to stress caused by damaging environmental insults. Physical wounding, toxins, reactive oxygen species and UV irradiation all induce cellular damage and thus disrupt tissue integrity. Mounting an appropriate response to these insults is essential for tissue repair and to prevent chronic cellular stress, which can lead to disease (Fulda et al., 2010). While much progress has been made to elucidate signalling pathways that seal wounds, remove damaged cells, promote regenerative proliferation or mediate patterning of regenerated tissue, little is known about how crosstalk between these pathways coordinates repair processes to restore homeostasis.

Studies on *Drosophila* progenitor organs called imaginal discs have provided deep insights into cellular adaptations to tissue stress. Surgical excision (Bryant, 1975; Haynie and Bryant, 1976; Katsuyama et al., 2015) or cell ablation induced by pro-apoptotic transgenes (Grusche et al., 2011; Herrera et al., 2013; Smith-Bolton et al., 2009) has revealed cellular responses that promote wound healing (Sun and Irvine, 2014; Kashio et al., 2014; Razzell et al., 2011). Disc size is restored by accelerated proliferation of cells proximal (Sustar et al., 2011; Bosch et al., 2008) and distal (Herrera et al., 2013) to the wound site. Lacking tissue-resident stem cells, fate plasticity displayed by parenchymal disc cells facilitates repatterning of replaced tissues (Herrera et al., 2013; Herrera and Morata, 2014; Repiso et al., 2013; Schuster and Smith-Bolton, 2015). In contrast, regeneration of the *Drosophila* adult midgut is driven by tissue-resident stem cells (Ohlstein and Spradling, 2006; Jiang et al., 2009; Osman et al., 2013; Staley and Irvine, 2010). Strikingly, while midgut and imaginal discs utilize stem cell-dependent and -independent repair processes, both tissues activate similar signalling pathways that underlie potentially highly conserved stress responses.

The c-Jun amino-terminal kinase (JNK)/mitogen-activated protein kinase (MAPK) cascade is one of the earliest pathways activated in damaged tissues and it is triggered by loss of epithelial polarity (Brumby and Richardson, 2003; Uhlirova et al., 2005; Igaki, 2009; Wu et al., 2010; Zhu et al., 2010), apoptosis (Ryoo et al., 2004; Shlevkov and Morata, 2012) or physical wounding (Bosch et al., 2005; Rämet et al., 2002; Lee et al., 2005). JNK regulates stress responses via activation of the transcription factor AP-1 (Eferl and Wagner, 2003), which comprises Jun and Fos homo- and heterodimers. JNK activation is required for cytoskeletal rearrangement during wound closure (Ríos-Barrera and Riesgo-Escovar, 2013; Bosch et al., 2005) and promotes elimination of damaged cells by injury-induced apoptosis (Bogoyevitch et al., 2010; Chen, 2012; Shlevkov and Morata, 2012; Luo et al., 2007; Moreno et al., 2002). Importantly, JNK drives compensatory proliferation to replace damaged tissues, through cell-autonomous (Bosch et al., 2008; Sun and Irvine, 2011; Grusche et al., 2011) and non-autonomous (Bergantinos et al., 2010; Mattila et al., 2005; Ryoo et al., 2004) mechanisms. A central question remaining unanswered is how these two different responses – proliferation and apoptosis – are brought into equilibrium downstream of JNK to restore tissue homeostasis.

Apoptotic JNK targets that facilitate clearing of damaged cells include the Diap1 inhibitors *reaper* (*rpr*), *head involution defective* (*hid*) and *p53* (Shlevkov and Morata, 2012; Luo et al., 2007; Moreno et al., 2002). Activation of *rpr*, *hid* and *p53* drives further activation of JNK via the initiator caspase Dronc (Shlevkov and Morata, 2012). JNK also activates the TNFα homologue Eiger (Pérez-Garijo et al., 2013), leading to activation of JNK in nearby cells (Pérez-Garijo et al., 2013; Bergantinos et al., 2010; Wu et al., 2010). This positive feedback could drive excessive cell elimination and therefore, needs to be restrained to prevent unlimited spatial propagation of pro-apoptotic JNK activity. It is not known how spatial constraints on JNK propagation are established.

Ludwig-Maximilians-University Munich, Faculty of Biology, Grosshaderner Strasse 2-4, Planegg-Martinsried 82152, Germany.

*Author for correspondence (classen@bio.lmu.de)

A.-K.C., 0000-0001-5157-0749

Received 1 November 2015; Accepted 23 June 2016

Development (2016) 143, 2907-2919 doi:10.1242/dev.132340

Importantly, apoptosis of damaged cells stimulates compensatory proliferation by JNK-dependent activation of growth pathways including Wnt/β-catenin, TFGβ/SMAD, Janus kinase/Signal transducer and activator of transcription (JAK/STAT), Hippo/Yorkie and EGF (Sun and Irvine, 2011, 2014; Wells et al., 2006; Kondo et al., 2006; Huh et al., 2004; Morata et al., 2011; Pastor-Pareja and Xu, 2013). While the requirement for these pathways differs depending on context (Smith-Bolton et al., 2009; Herrera et al., 2013; Fan and Bergmann, 2008), many have been implicated in metazoan responses to stress (Sun and Irvine, 2014; Pahlavan et al., 2006; Chen, 2012). Importantly, prevention of apoptosis in damaged cells causes sustained proliferative signalling and eventual tumour formation in *Drosophila* (Kondo et al., 2006; Perez-Garijo et al., 2004, 2009; Ryoo et al., 2004; Huh et al., 2004; Martin et al., 2009), emphasizing how strongly apoptotic, survival and proliferative signals need to be balanced to re-establish normal tissue size.

Current models propose that JAK/STAT signalling is a major mediator of compensatory, cancerous and developmental proliferation. Cytokine-like ligands in *Drosophila* are encoded by *upd1* (*unpaired 1*), *upd2* and *upd3* and signal through conserved pathway components encoded by single genes, specifically the receptor Domeless (Dome), the Janus kinase Hopscotch (Hop) and the transcription factor Stat92E (Arbouzova and Zeidler, 2006). As in mammals, JAK/STAT plays diverse roles in fly development by regulating haemocyte activation (Myllymäki and Rämet, 2014), appendage patterning (Ayala-Camargo et al., 2013, 2007; Johnstone et al., 2013) and stem cell maintenance (Gregory et al., 2008). A proliferative function for JAK/STAT was suggested by early studies of tissue growth during disc development (Bach et al., 2003; Tsai and Sun, 2004; Mukherjee et al., 2005). Subsequently, JAK/STAT has been widely implicated in promoting proliferation of neoplastic cells (Classen et al., 2009; Wu et al., 2010; Davie et al., 2015; Bunker et al., 2015; Amoyel et al., 2014) and aberrant non-autonomous proliferation of wild-type cells in fly models of tumorigenesis (Vaccari and Bilder, 2005; Herz et al., 2006; Moberg et al., 2005). Activation of Upd gene transcription upon tissue damage has been linked to compensatory proliferation in imaginal discs and adult guts (Jiang et al., 2009; Pastor-Pareja et al., 2008; Katsuyama et al., 2015; Wu et al., 2010; Lin et al., 2009; Bunker et al., 2015; Santabárbara-Ruiz et al., 2015). Other studies suggest that JAK/STAT is involved in cell competition, where signalling either promotes 'winner' cell state (Schroeder et al., 2013; Rodrigues et al., 2012) or compensatory proliferation in response to 'loser' cell elimination (Kolahgar et al., 2015).

Despite this wealth of work, little is known about target genes mediating proliferative JAK/STAT function. In fly tumours, STAT-responsive enhancers have been mapped (Davie et al., 2015), but few target genes regulating tissue size have been described (Tsai and Sun, 2004; Betz et al., 2008; Hasan et al., 2015). However, several studies suggest that developmental functions of JAK/STAT are mediated by the transcriptional repressors Chinmo (Flaherty et al., 2010), Zfh1 (Ohayon et al., 2009; Leatherman and Dinardo, 2008) and Zfh2 (Perea et al., 2013; Guarner et al., 2014; Ayala-Camargo et al., 2013).

We wanted to better understand the precise role of JAK/STAT in cellular adaptations to stress and to gain further insight into how JAK/STAT might regulate compensatory proliferation after tissue damage. Because JAK/STAT is required for regeneration in tissues as diverse as the grasshopper leg to the mouse liver (Yamada et al., 1997; Bando et al., 2013; Cressman et al., 1996; Li et al., 2002; Wuestefeld et al., 2003; Zhao et al., 2014), dissecting the function of this highly conserved pathway is essential for our understanding of regenerative processes. To achieve this, we employed an imaginal disc model of tissue stress, which utilizes ectopic expression of the TNFα homologue Eiger (Smith-Bolton et al., 2009) (Fig. S1), triggering JNK activation (Igaki and Miura, 2014; Andersen et al., 2015) and apoptosis (Fig.S1D-D‴). This model has been previously used to study tissue regeneration in response to local cell ablation (Herrera et al., 2013; Smith-Bolton et al., 2009). Expression of Eiger induces multiple hallmarks of local and systemic stress responses, such as compensatory proliferation and dILP8-induced developmental delay (Fig. S1E,G) (Smith-Bolton et al., 2009). Because Eiger induces tissue stress in wild-type discs, it represents an ideal model to distinguish JAK/STAT functions in physiological stress from secondary effects incurred by developmental patterning or tumorigenic models. Instead of promoting compensatory proliferation, we found that JAK/STAT promotes survival of JNK-signalling cells, thereby acting as a central regulator of injury-induced apoptosis to restrain excessive tissue damage and facilitate initiation of compensatory responses.

RESULTS

Eiger-mediated JNK activation enables functional studies of JNK-dependent stress responses

We expressed Eiger under the control of *rotund* (*rn*)-*GAL4*, which drives expression in the wing disc pouch, fated to give rise to the future wing blade. We induced *eiger* expression on developmental day 7 and temporally limited *UAS-eiger* expression to 40 h by using a temperature-sensitive GAL80 repressor (Fig. S1A-C). In agreement with previous studies (Herrera et al., 2013; Smith-Bolton et al., 2009), we observed extensive cell ablation in discs (Fig. S1E-E′), which gave rise to a 50% reduction in adult wing size (Fig. S1H). G-trace lineage labelling (Evans et al., 2009) of *rn-GAL4*-expressing cells followed by FACS analysis revealed that about 85% of *rn-GAL4* lineage cells were eliminated after 40 h of Eiger stimulation (Fig. 1A,A′, Fig. S2A-A″). This correlated with an induction of a 2 day developmental delay at the larval-pupal transition (Fig. S1G).

In agreement with Eiger triggering JNK activation (Igaki and Miura, 2014), we found that Eiger-stimulated discs broadly activate the JNK-responsive *TRE* reporter (Fig. 1C) (Chatterjee and Bohmann, 2012). The *TRE* reporter was specifically activated at the wound site, whereas reporter activity is completely absent in control discs (Fig. 1B,C). Consistent with non-autonomous activation of JNK by Eiger (Pérez-Garijo et al., 2013) and tissue damage (Bosch et al., 2005; Herrera et al., 2013; Wu et al., 2010), *TRE* activation extended beyond a G-trace-labelled domain, in which *eiger* expression was induced (Fig. 1C and Fig. 2F). FACS analysis demonstrated that while 4.5% of cells in the disc belonged to the surviving *rn-GAL4* lineage, 29% of cells in the disc activated *TRE-GFP* (Fig. S2A-A′,B-B′).

We first wanted to quantify cell proliferation in Eiger-stimulated discs near the wound site, as well as in the whole disc between 0 h (R0) and 48 h (R48) into the recovery period after the end of cell ablation (Fig. S1A,E-E″). We used an image segmentation algorithm (Fiji) to specifically measure total disc size, the size of the surviving *rn-GAL4* lineage labelled by G-trace, the number of mitotic cells marked by phospho-Histone 3 (pH3) or the number of cells in S-phase marked by BrdU incorporation (Fig. 1D-G, Fig. S1F). We found that at R0, G-trace-labelled cells in the pouch account for about 3% of the total disc volume (Fig. 1D). This is in close agreement with FACS measurements (4.5%, Fig. S2A′), which also detect an additional subset of G-trace-labelled cells in

Development (2016) 143, 2907-2919 doi:10.1242/dev.132340

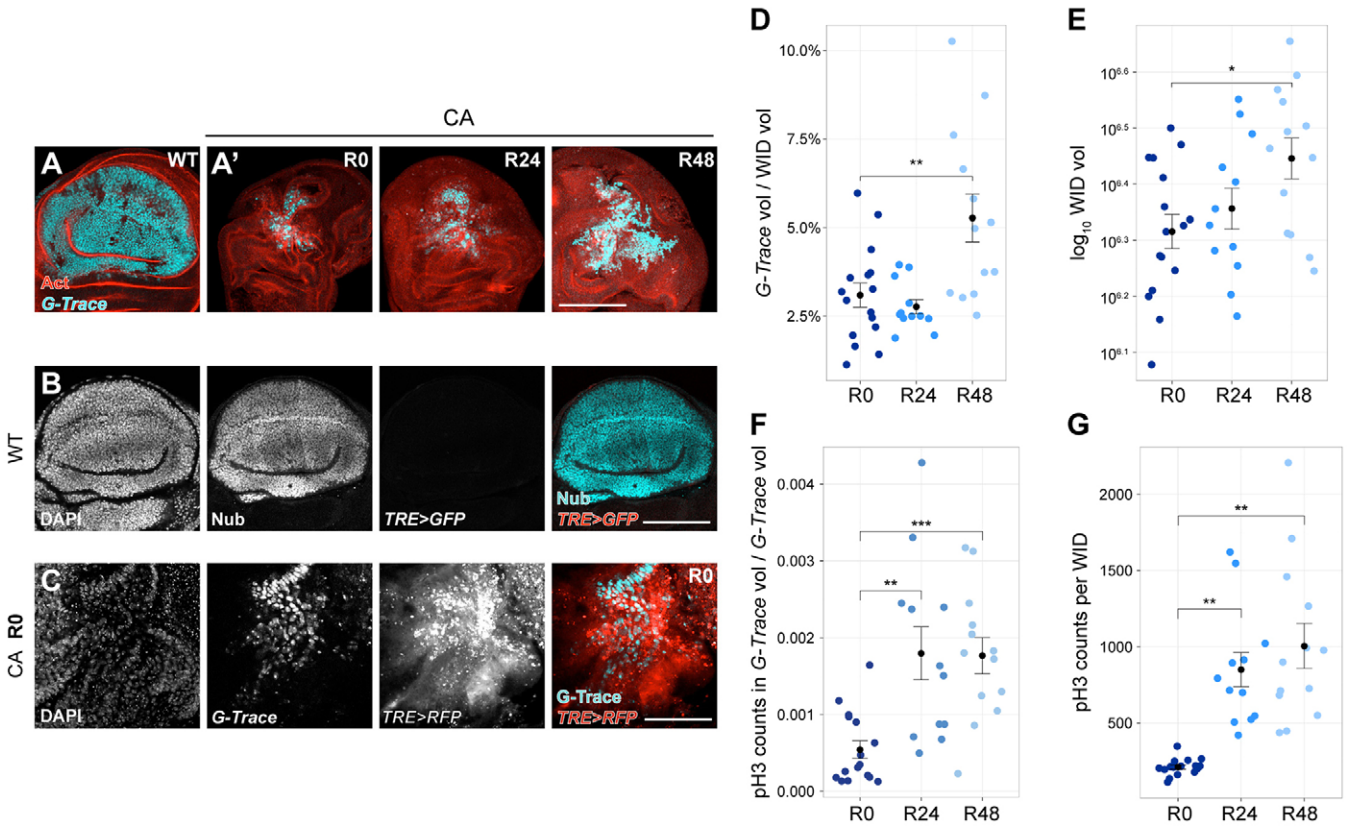

Fig. 1. Eiger expression enables functional studies of JNK stress responses. (A) G-trace labelling (cyan) visualizes the *rotund* (*rn*)*GAL4* cell lineage in wing discs. Actin labelling is red. (A′) Progeny of *rn-GAL4* G-trace-labelled cells (cyan) after 40 h of Eiger-mediated cell ablation (CA) at recovery points R0, R24, R48 h. (B) Wing pouch expressing the JNK reporter *TRE>GFP* (red in overlay), stained for DAPI and Nubbin (cyan in overlay) visualizing a lineage similar to *rn-GAL4*-derived cells. (C) Wing pouch after cell ablation (CA) expressing *TRE*>RFP (red in overlay) containing *rn-GAL4* G-trace-labelled cells (cyan in overlay) stained for DAPI. (D) Volume occupied by *rn-GAL4* G-trace-labelled cells and (E) total wing imaginal disc (WID) volumes at recovery time points R0, R24 and R48. (F) Normalized pH3-positive mitotic events within *rn-GAL4* G-trace-labelled volume and (G) within total disc volumes at R0, R24, R48. Graphs display mean±s.e.m. for R0, *n*=16; R24, *n*=12; R48, *n*=13 discs. *U*-tests were performed to test for statistical significance (*P<0.05, **P<0.01, ***P<0.001). Scale bars: 100 µm.

the notum. This analysis verified that volume quantifications of cell populations in Fiji accurately approximate cell counts. Our analysis revealed a marked increase in cell proliferation between R0 and R24, both near the wound site (Fig. 1F), as well as in the entire disc (Fig. 1G, Fig. S2E). Mitotic rates do not increase further between R24 and R48 (Fig. 1F,G). When we quantified the volume of the total disc and that of the G-trace-labelled population, we found that they increased in size by 36% and 126%, respectively (Fig. 1D,E).

While cell ablation can be induced more efficiently by expression of pro-apoptotic transgenes, such as *UAS-reaper* (Herrera et al., 2013), we did not observe broad activation of JNK in this context (Fig. S2C,D). Because Eiger-stimulated discs displayed broad activation and provided genetic access to JNK-signalling cells, we utilized expression of Eiger to investigate the role of JAK/STAT in JNK-mediated responses to tissue stress.

JAK/STAT is activated in response to Eiger-induced tissue damage

To understand if JAK/STAT plays a role in imaginal disc regeneration, we analysed JAK/STAT activity in response to *eiger* expression. JAK/STAT activation can be visualized using the *10xSTAT-dGFP* reporter (Bach et al., 2007), which is almost undetectable in wild-type discs (Fig. 2A). Analysis of the *10xSTAT-dGFP* reporter revealed that JAK/STAT is upregulated in response to *eiger* expression induced at day 5 or day 7 of development (Fig. 2B,C). Reporter activation can also be observed upon *reaper* expression, suggesting that stress induced by ectopic cell death is sufficient to cause JAK/STAT activation (Fig. S3E). Importantly, in Eiger-stimulated discs, JAK/STAT activation was detected beyond the pouch periphery and thus extended beyond JNK domains marked by *TRE* activity (Fig. 2F). JAK/STAT signalling declined within the following 24 h suggesting that it is downregulated after *eiger* expression ceased (compare Fig. S3A-C with Fig. S3B′-C′). We furthermore examined JAK/STAT activation when *eiger* was induced at later stages of development. Surprisingly, JAK/STAT activity was almost undetectable when *eiger* was induced at day 8 (Fig. 2D, Fig. S3D-D′).

Unpaired ligands are upregulated upon Eiger-induced tissue damage

Previous reports and our studies demonstrate that the JAK/STAT ligands *upd1*, *upd2* and *upd3* are transcriptionally upregulated in response to stress from physical injury (Katsuyama et al., 2015; Pastor-Pareja et al., 2008) or tumorous growth (Wu et al., 2010; Bunker et al., 2015), indicating that pathway upregulation may be driven by JNK-dependent Upd gene transcription. We found that transcription of Upd genes is highly elevated in Eiger-stimulated discs, whereas transcription of *dome*, *hop* and *Stat92E* is not (Fig. 2E). Recapitulating the decline in *10xSTAT-dGFP* activity in response to *eiger* induction at day 8, Upd gene transcription was

Development (2016) 143, 2907-2919 doi:10.1242/dev.132340

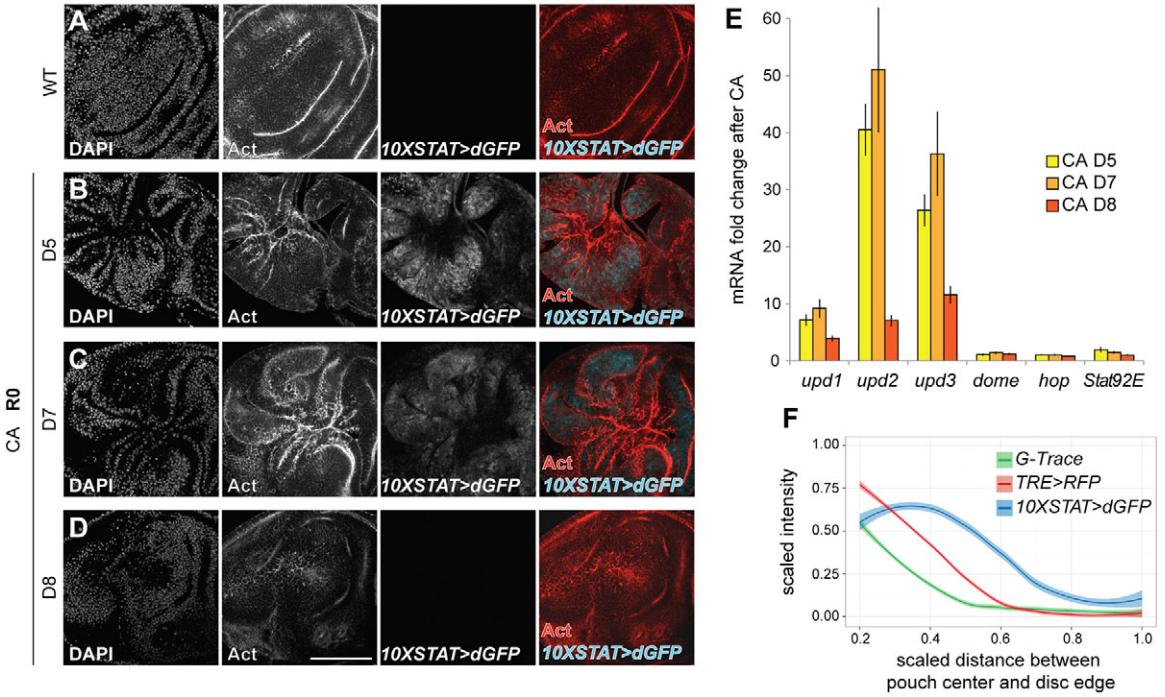

Fig. 2. JAK/STAT is activated in response to tissue damage. (A) Wing disc expressing the JAK/STAT-reporter *10XSTAT>dGFP* (cyan in overlay) stained for DAPI and Actin (red in overlay). (B-D) Wing pouch after cell ablation (CA) induced at day 5 (B), day 7 (C) or day 8 (D). Discs were stained for DAPI, Actin (red in overlay) and express *10XSTAT>dGFP* (cyan in overlay). (E) qRT-PCR analysis of *upd1*, *upd2*, *upd3*, *dome*, *hop* and *Stat92E* transcripts after cell ablation (CA) induced at day 5, day 7 or day 8. Fold induction relative to unablated controls is reported. Graphs display mean±s.e.m. for $n \geq 3$ biological replicates. (F) Fluorescence intensity of *rn-GAL4* G-trace (n=5 discs), *TRE>RFP* (n=6 discs) and *10XSTAT>dGFP* (n=12 discs) reporter signals at R0. Intensity plots are scaled to maximum measured values; interpolated averages are reported as a function of relative positions between pouch centre and disc edge. Graphs display interpolated mean±s.e.m. Scale bars: 100 µm.

strongest at day 5 and day 7 but decreased by more than half when *eiger* was induced at day 8 (Fig. 2E).

Loss of JAK/STAT activation at day 8 was not due to a decline in Eiger-mediated JNK activation, because *TRE* activity was as strong on day 8 as on day 7 (Fig. S3F,G). This suggests that even though JAK/STAT activation coincides with JNK activity (Katsuyama et al., 2015; Pastor-Pareja et al., 2008), JNK alone may not be sufficient to stimulate this pathway. This is supported by broader activation of JAK/STAT compared with JNK (Fig. 2F). Strikingly, the failure to activate JAK/STAT at late developmental stages correlated with a pronounced decline in the ability of larvae to induce a developmental delay at the larval-pupal transition (Fig. S3H) and with a strong reduction in recovered adult wing size (Fig. S3I). These correlations suggest that JAK/STAT may be a crucial mediator of JNK-induced compensatory responses in imaginal discs.

JAK/STAT activity is not required for compensatory proliferation

JAK/STAT has been reported to play a role in promoting cell proliferation in wild-type (Bach et al., 2003; Tsai and Sun, 2004; Mukherjee et al., 2005), tumorous (Classen et al., 2009; Wu et al., 2010; Davie et al., 2015; Bunker et al., 2015; Amoyel et al., 2014) and surgically injured discs (Katsuyama et al., 2015). To test whether JAK/STAT is generally required to drive compensatory proliferation, we quantified mitotic events after Eiger stimulation in discs with impaired JAK/STAT signalling. We genetically reduced JAK/STAT activity by two approaches: (1) we reduced gene dosage of JAK/STAT components in the entire animal by heterozygosity for $dome^{G0441}$, hop^{34} and $Stat92E^{85C9}$ alleles or (2) we interfered with JAK/STAT signalling exclusively in *eiger*-expressing cells through expression of RNAi constructs targeting JAK/STAT components (Fig. S5A), a dominant-negative *dome* ($dome^{\Delta cyt}$) or the inhibitor *Socs36E* under the control of *rn-GAL4-tubGAL80^{ts}*.

Strikingly, even though 50% of the tissue in Eiger-stimulated discs activated JAK/STAT (Fig. 2B,C), discs heterozygous for $dome^{G0441}$, hop^{34} and $Stat92E^{85C9}$ alleles did not show any evidence of a reduction in mitotic events or total disc size (Fig. 3A-F). Instead, we observed a mild increase in Eiger-stimulated discs heterozygous for hop^{34}. These results are the opposite to what we would expect if JAK/STAT regulated compensatory proliferation. We thus wanted to confirm these findings by interfering with JAK/STAT specifically in Eiger-stimulated cells. *rn-GAL4*-driven co-expression of *dome-RNAi*, $dome^{\Delta cyt}$ or *Socs36E* did not reduce the number of mitotic events within surviving *eiger*-expressing cells (Fig. 3G-K). Instead, mitotic rates slightly increased, whereas they remained unchanged in the rest of the disc (Fig. 3K, Fig. S4A,C). Importantly, effects on *eiger*-expressing cells co-expressing transgenic constructs are strongest at R0 but decline as GAL4 activity decreased (Fig. 3K). Together, our results strongly argue against the previously assigned role of JAK/STAT in directly promoting compensatory proliferation in response to stress.

JAK/STAT is required for survival of JNK-signalling cells

While the total disc size of Eiger-stimulated discs was similar to that of discs with genetically impaired JAK/STAT activity (Fig. 3F, Fig. S4D), we were surprised to notice that the number of

Development (2016) 143, 2907-2919 doi:10.1242/dev.132340

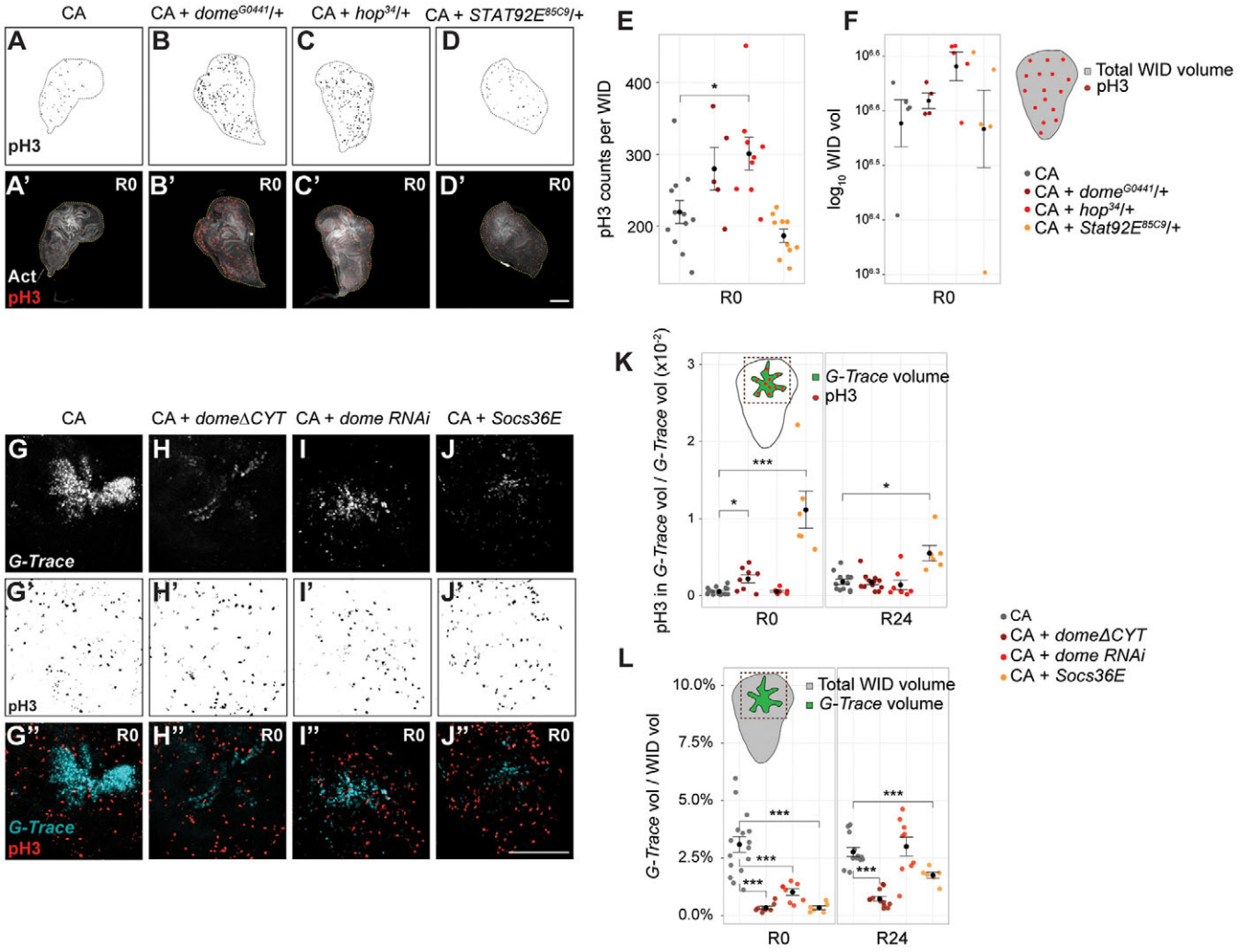

Fig. 3. JAK/STAT is not required for compensatory proliferation. (A) Wing disc after cell ablation (CA) stained for pH3 (A, red in A′, Actin in grey). (B-D) Wing disc heterozygous for *dome*^{G0441} (B,B′), *hop*^{34} (C,C′) or *Stat92E*^{85C9} (D,D′) after cell ablation (CA) stained for pH3 (B-D, red in B′-D′; Actin in grey). (E) pH3 events per disc or (F) total wild-type disc volume (n=12) and discs heterozygous for *dome*^{G0441} (n=5), *hop*^{34} (n=9), or *Stat92E*^{85C9} (n=10) after cell ablation (CA). (G-J) Wing pouch containing surviving *rn-GAL4* G-trace-labelled cells (G-J, cyan in G″-J″), stained for pH3 (G′-J′, red in G″-J″). A wild-type disc (G) and discs with *rn-GAL4*-mediated co-expression of *dome*$^{\Delta cyt}$ (H), *dome-RNAi* (I) or *Socs36E* (J) in *eiger*-expressing cells are shown. (K) Normalized pH3 events within *rn-GAL4* G-trace-labelled volume and (L) relative *rn-GAL4* G-trace-labelled volume per disc at R0 and R24 in ablated discs (CA) (R0, n=16; R24, n=12 discs) or with *rn-GAL4*-mediated co-expression of *dome*$^{\Delta cyt}$ (R0, n=8; R24, n=12 discs), *dome-RNAi* (R0, n=8; R24, n=9 discs), *Socs36E* (R0, n=6; R24, n=6 discs) in *eiger*-expressing cells. Graphs display mean±s.e.m. *U*-tests were performed to test for statistical significance (*P<0.05, **P<0.01, ***P<0.001). Scale bars: 100 µm.

G-trace-labelled cells that survived *eiger* expression was dramatically reduced when JAK/STAT signalling was inhibited. Specifically, we found that expression of *dome-RNAi*, *dome*$^{\Delta cyt}$ or *SOCS36E* caused a 3- to 10-fold reduction in the volume of G-trace-labelled populations (Fig. 3L, Fig. S4B).

These observations suggested that more *eiger*-expressing cells die when JAK/STAT signalling is impaired. Indeed, we observed a 2-fold increase in the volume positive for activated Caspase-3 if JAK/STAT activity was exclusively reduced in *eiger*-expressing cells (Fig. 4A-E) and up to a 10-fold increase in the volume of Eiger-stimulated discs heterozygous for *dome*^{G0441}, *hop*^{34} or *Stat92E*^{85C9} (Fig. 4F-I). The more pronounced effect observed for heterozygous tissues likely arises as a result of the tissue-wide reduction of JAK/STAT activity in this background. Reduction was also achieved in domains that display JAK/STAT and JNK activation but are located outside of the *rnGAL4* lineage (Fig. 1C, Fig. 2B,C,F). Importantly, genetic reduction of JAK/STAT in developing wild-type discs under the same conditions does not cause any elevation of apoptosis (Fig. S5B-E). Combined, these data highlight a specific role for JAK/STAT as an important mediator of cell survival, specifically in JNK-signalling cells.

JAK/STAT activity suppresses activation of JNK signalling

To understand how JAK/STAT promotes cell survival, we tested if genetically reducing JAK/STAT activity causes further elevation of JNK, which could divert JNK-dependent compensatory responses towards apoptosis. To this end, we monitored JNK activity using *TRE* reporters in *eiger*-expressing discs heterozygous for *dome*^{G0441}, *hop*^{34} and *Stat92E*^{85C9} alleles. Our results suggested that after cell ablation, 14% of the wing pouch area activated the *TRE* reporter (Fig. 4J,N). In Eiger-stimulated discs heterozygous for *dome*^{G0441}, *hop*^{34} and *Stat92E*^{85C9}, we observed a 2- to 3-fold increase in the area positive for *TRE* activation (Fig. 4K-N). These results indicate that reduction of JAK/STAT signalling promotes non-autonomous expansion of JNK signalling beyond *eiger*-expressing cells and that this may underlie the observed increase

Development (2016) 143, 2907-2919 doi:10.1242/dev.132340

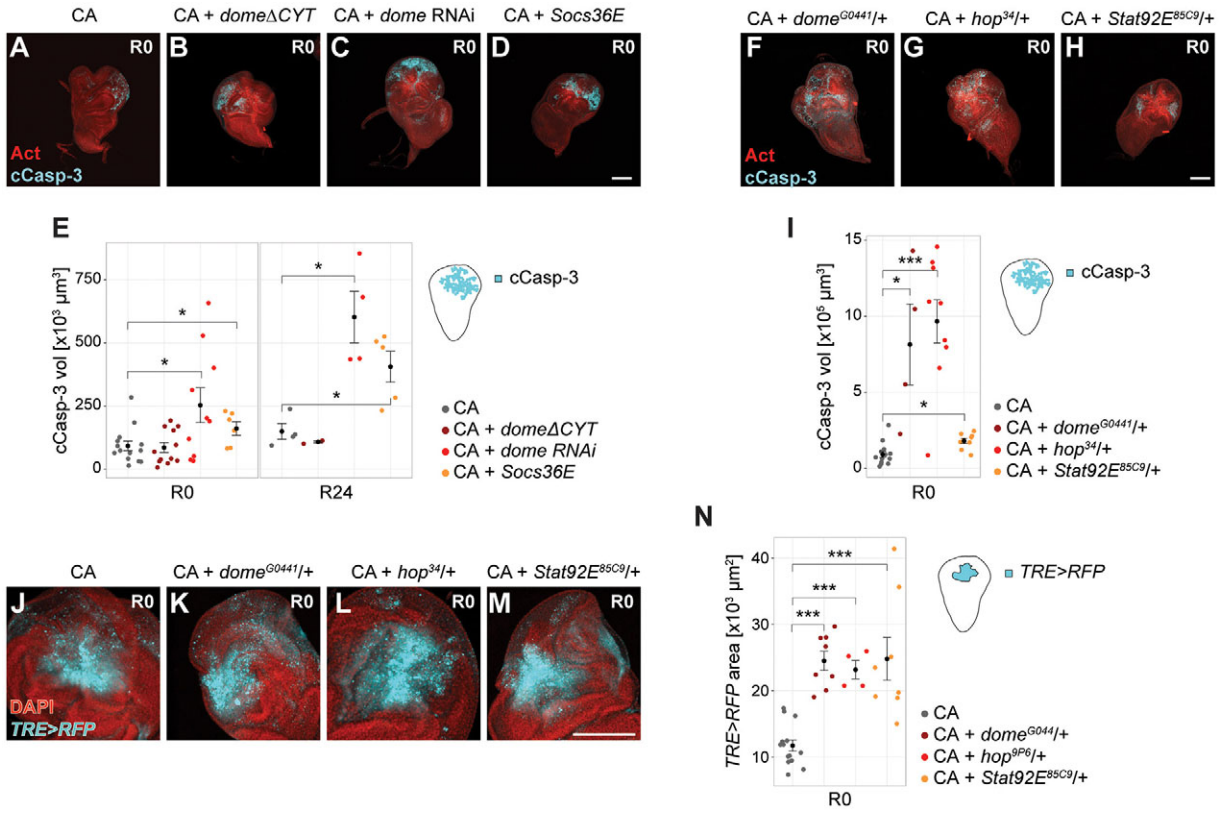

Fig. 4. JAK/STAT is required for survival of Eiger-stimulated cells. (A-D) Wing disc after cell ablation (CA) (A) and with *rn-GAL4*-mediated co-expression of *dome*$^{\Delta cyt}$ (B), *dome-RNAi* (C) or *Socs36E* (D) in *eiger*-expressing cells stained for cleaved Caspase-3 to visualize apoptotic cells (cyan) and Actin (red). (E) Cleaved Caspase-3 volume in ablated discs (CA; R0, *n*=15; R24, *n*=4 discs) or with *rn-GAL4*-mediated co-expression of *dome*$^{\Delta cyt}$ (R0, *n*=12; R24, *n*=3 discs), *dome-RNAi* (R0, *n*=10; R24, *n*=4 discs) or *Socs36E* (R0, *n*=6; R24, *n*=6 discs) in *eiger*-expressing cells at R0 and R24. (F-H) Ablated discs heterozygous for *dome*^{G0441} (F), *hop*^{34} (G) or *Stat92E*^{85C9} (H) stained for cleaved Caspase-3 (cyan) and Actin (red) at R0. (I) Quantification of cleaved Caspase-3-positive volume per disc after cell ablation (CA) (*n*=12 discs) or in discs heterozygous for *dome*^{G0441} (*n*=4 discs), *hop*^{34} (*n*=9 discs), or *Stat92E*^{85C9} (*n*=8 discs) at R0. (J-M) Disc expressing the JNK reporter *TRE>RFP* (cyan) after cell ablation (CA) (J) or if heterozygous for *dome*^{G0441} (K), *hop*^{34} (L) or *Stat92E*^{85C9} (M) at R0. (N) Quantification of *TRE>RFP*-positive area per disc after cell ablation (CA) (*n*=14 discs) and in discs heterozygous for *dome*^{G0441} (*n*=8 discs), *hop*^{34} (*n*=4 discs), or *Stat92E*^{85C9} (*n*=8 discs). Graphs display mean±s.e.m. *U*-tests were performed to test for statistical significance (**P*<0.05, ***P*<0.01, ****P*<0.001). Scale bars: 100 µm.

in the apoptotic index in JAK/STAT-impaired Eiger-stimulated discs (Fig. 4A-I).

Our observations prompted two important predictions. First, broad activation of JNK in JAK/STAT-impaired discs suggested that JAK/STAT acts as a suppressor of JNK signalling. Repression of JNK by JAK/STAT could either be mediated by direct transcriptional effects on JNK core components, or indirectly, by suppression of apoptosis and prevention of Dronc-driven positive feedback activation of JNK. This mechanism would restrain non-autonomous activation of JNK, excessive apoptosis and tissue damage. A second prediction implies that interfering with JAK/STAT increases the extent of tissue damage due to elevation of cell death. Thereby, the ability of discs to mount an appropriate regenerative response is reduced as cells required to drive regenerative responses are eliminated by excessive cell death.

A survival-promoting function of JAK/STAT is mediated by Zfh2

We did not find any evidence that negative JNK regulators are transcriptionally activated by Stat92E. We therefore wanted to understand if JAK/STAT regulates cell survival by impinging on pro-apoptotic JNK target genes *rpr* and *hid*, which act in combination with *grim* as inhibitors of IAP (inhibitor of apoptosis) proteins. To this end, we first performed a bioinformatic Clover analysis of the promoter regions of *rpr*, *hid* and *grim* using highly stringent parameter selections (Frith et al., 2004). As previously suggested (Shlevkov and Morata, 2012; Luo et al., 2007; Moreno et al., 2002), we identified multiple AP-1 binding motifs associated with these loci (Fig. S7A, data not shown). In agreement with studies on JNK-induced apoptosis (Shlevkov and Morata, 2012; Luo et al., 2007; Moreno et al., 2002), we specifically observed induction of *hid* expression in Eiger-stimulated discs (Fig. 5A). The mild increase in *hid* levels is likely to be an underestimate because *eiger*-expressing cells make up only 4.5% of the entire disc used for qRT-PCR analysis (Fig. S2A,A′). *Eiger*-expressing discs heterozygous for *Df(3L)H99*, a deficiency removing *rpr*, *hid* and *grim* loci, displayed a pronounced ‘undead cell’ phenotype (Fig. S6A,B) (Perez-Garijo et al., 2009; Martin et al., 2009; Kondo et al., 2006), suggesting that upregulation of *hid* contributes to Eiger-mediated cell death. While one previous study reports that Eiger-mediated induction of apoptosis is independent of *hid* activation (Igaki et al., 2002), we suggest that the small adult eye phenotype observed upon *eiger* co-expression with the strong apoptosis inhibitor p35 is a consequence of epithelial tissue architecture disruption rather than a failure to prevent Eiger-induced cell death (Fig. S6L). Together, previous reports and our results support the notion that induction of cell death in *eiger*-

Development (2016) 143, 2907-2919 doi:10.1242/dev.132340

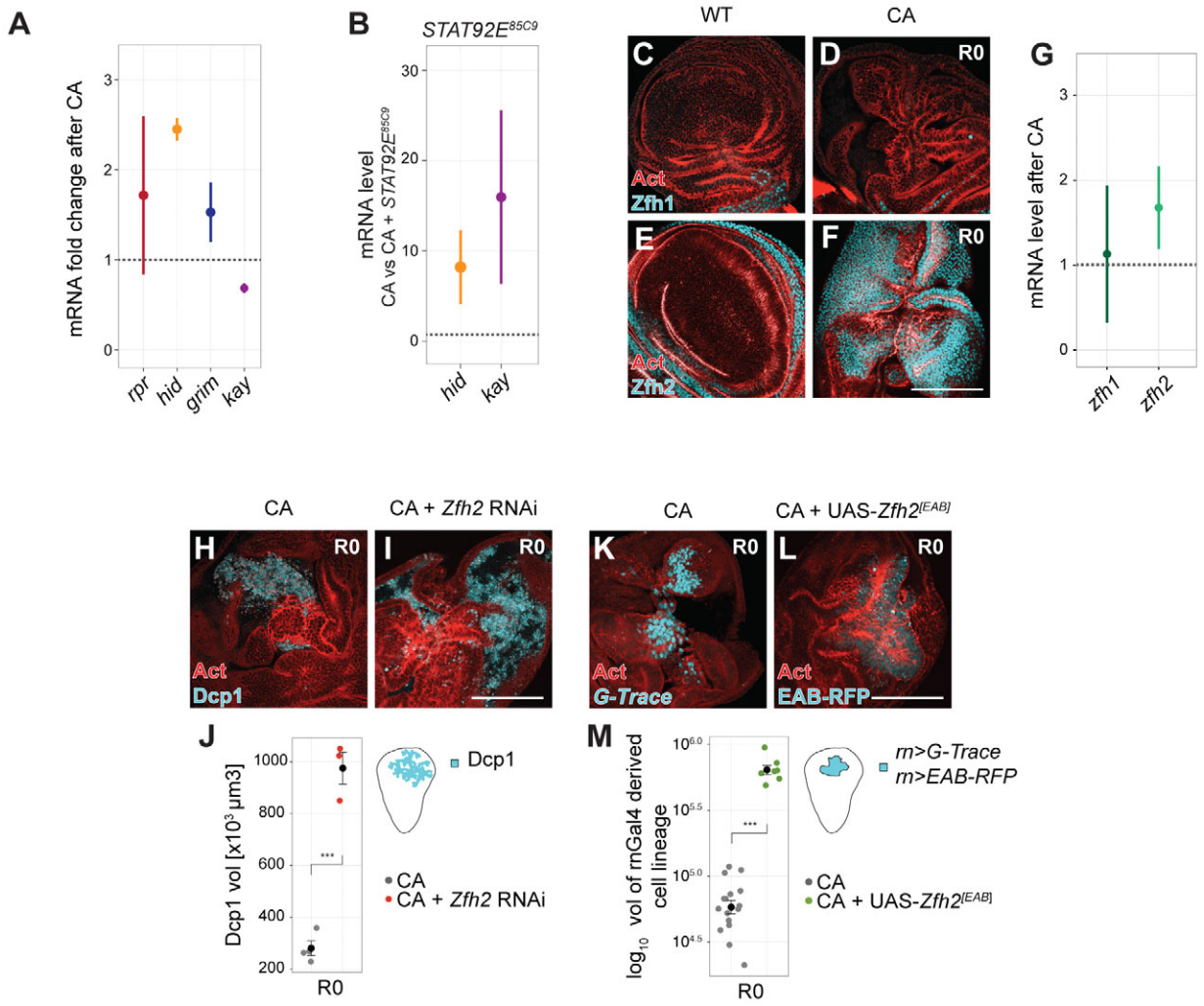

Fig. 5. A survival-promoting function of JAK/STAT is mediated by Zfh2. (A) qRT-PCR analysis of *rpr*, *hid*, *grim* and *fos* (*kay*) transcripts at R0. Fold induction relative to unablated discs is reported. Each graph shows mean±s.e.m. for $n \geq 3$ biological replicates. (B) qRT-PCT analysis of *hid* and *kay* at R0 in Eiger-expressing discs heterozygous mutant for *Stat92E*^{85C9}. Fold induction relative to ablated discs. Each graph shows mean±s.e.m. for $n=2$ biological replicates. (C-F) Unablated discs (C,E) and ablated discs (D,F) stained for Zfh1 (C,D) or Zfh2 (E,F) at R0. (G) qRT-PCR analysis of *zfh1* and *zfh2* transcripts at R0. Fold induction relative to unablated discs is reported. Each graph shows mean±s.e.m. for $n=3$ biological replicates. (H,I) Disc after cell ablation (H) or with *rn-GAL4*-mediated co-expression of *zfh2-RNAi* (I) in *eiger*-expressing cells stained for Dcp-1 to visualize apoptotic cells (cyan) and Actin (red) at R0. (J) Dcp1-positive volume per disc after cell ablation (CA) ($n=4$ discs) or in discs with *rn-GAL4*-mediated co-expression of *zfh2-RNAi* ($n=3$ discs) in *eiger*-expressing cells at R0. (K,L) Disc after cell ablation (K) or discs with *rn-GAL4*-mediated co-expression of *UAS-zfh2* (L) in *eiger*-expressing cells stained for Dcp-1 (cyan) and Actin (red) at R0. (M) *rn-GAL4* G-trace-labelled volume in ablated discs ($n=16$ discs) and RFP-labelled volume in discs with *rn-GAL4*-mediated co-expression *UAS-Zfh2*$^{[EAB]}$ ($n=7$ discs) in *eiger*-expressing cells at R0. Graphs display mean±s.e.m. *U*-tests were performed to test for statistical significance (*$P<0.05$, **$P<0.01$, ***$P<0.001$). Scale bars: 100 µm.

expressing discs is specifically mediated by AP-1/JNK-dependent activation of *hid*.

Strikingly, our Clover analysis also revealed multiple, highly clustered mammalian ZEB1-binding motifs the *hid* promoter (Fig. S7A) as well as in the promoter of the *kay* gene coding for the AP-1 component dFos (Fig. S7B). ZEB1 binding motifs localized to highly conserved DNA sequences as shown by mVISTA analysis (Frazer et al., 2004; Bray et al., 2003) and to open chromatin regions, likely representing regulatory elements, as demonstrated by overlays with previously published ATAC-seq data sets (Fig. S7) (Davie et al., 2015). ZEB proteins are homologous to *Drosophila* Zfh1 and Zfh2 (Zinc-finger homeobox) proteins, which act as transcriptional repressors (Postigo et al., 1999; Postigo and Dean, 1999). Both Zfh1 and Zfh2 were previously identified to be downstream effectors of JAK/STAT (Leatherman and Dinardo, 2008; Ayala-Camargo et al., 2013). This is reflected by Zfh2 expression mirroring JAK/STAT activation patterns in developing wing discs (Fig. 5E) (Ayala-Camargo et al., 2013) and the ability of JAK/STAT to induce Zfh2 expression *de novo* (Fig. S6C,D). We hypothesized that *Drosophila* ZEB proteins could directly mediate repression of *kay* in Eiger-stimulated discs (Fig. 5A), thereby restraining JNK activation to promote cell survival. At the same time, ZEB proteins could compete with AP-1 for transcriptional repression of *hid*, thereby limiting AP-1/Hid-induced apoptosis to promote cell survival. Indeed, in *eiger*-expressing discs heterozygous for *Stat92E*^{85C9}, the upstream regulator of Zfh proteins, we observed strong upregulation of *hid* and *kay* expression compared with discs expressing *eiger* alone (Fig. 5B).

To first understand if Zfh1 or Zfh2 expression was altered in tissue damage, we performed immunofluorescence and qRT-PCR

Development (2016) 143, 2907-2919 doi:10.1242/dev.132340

analysis on Eiger-stimulated discs. We found that levels of Zfh2, but not Zfh1, are elevated in response to *eiger* expression (Fig. 5C-F). Zfh2 upregulation occurred specifically in regions with high levels of JAK/STAT activation (compare Fig. 2B,C with Fig. 5F). In addition, we found that transcripts of *zfh2* but not of *zfh1* were elevated (Fig. 5G). The observed mild increase in *zfh2* transcription represents a strong underestimate, as cells expressing *zfh-2 de novo* make up only a small portion of entire imaginal discs used for qRT-PCR analysis. In agreement with Zfh2 being a JAK/STAT effector, heterozygosity for $STAT92E^{85C9}$ reduces Zfh2 expression in Eiger-stimulated discs (Fig. S6E-G).

To test if Zfh2 in Eiger-stimulated discs is required to promote JAK/STAT-dependent survival by repressing *hid* and *kay* transcription, we performed genetic experiments to reduce or increase Zfh2 function. We found that expression of an RNAi construct targeting *zfh2* (Fig. S6H) increased apoptosis in *eiger*-expressing discs almost 4-fold (Fig. 5H-J). In contrast, overexpression of *UAS-zfh2* strongly promoted survival of *eiger*-expressing cells and resulted in a 10-fold increase in the size of surviving *rn-GAL4*-derived cell populations (Fig. 5K-M). While we found that Zfh1 levels were not upregulated in response to stimulation with Eiger, overexpression of *zfh1* also promoted survival of *eiger*-expressing cells, even phenocopying overexpression of the strong apoptosis inhibitor p35 (Fig. S6I-L). The survival-promoting function of either Zfh1 or Zfh2 suggests that both proteins can induce potent survival signals in stressed tissues, similar to developmental contexts (Ohayon et al., 2009; Guarner et al., 2014).

JAK/STAT activity prevents excessive tissue damage in response to tissue stress

We predicted that interfering with JAK/STAT signalling and therefore with Zfh2 function, increases the extent of tissue damage incurred by Eiger due to elevation of cell death. Consistent with these predictions, we found that Eiger-stimulated discs with genetically reduced JAK/STAT activity developed into significantly smaller adult wings (Fig. 6A,B). Expression of $dome^{\Delta cyt}$, *Socs36E* or RNAi constructs targeting multiple pathway components, including *zfh2*, as well as heterozygosity for $dome^{G0441}$, hop^{34} and $Stat92E^{85C9}$, caused a significant drop in adult wing size index by 30-90% (Fig. 6B). Importantly, genetic downregulation of JAK/STAT in wild-type discs at day 7 does not cause a comparable reduction in wing size (Fig. S8A), emphasizing that the survival-promoting function of JAK/STAT is specifically required during tissue stress responses.

Notably, *rn-GAL4*-driven overexpression of *upd1*, *upd2* or *zfh2* in *eiger*-expressing cells did not increase adult wing size (Fig. 6B). Extra Upd may not translate into JAK/STAT hyperactivation, because of pathway saturation in *eiger*-expressing cells. While *zfh2* overexpression promoted cell survival, it did not rescue other defects such as loss of epithelial polarity (Fig. 5L), which interferes with wing morphogenesis.

To test whether JAK/STAT was also required for stress responses induced by physical wounding, we analysed adult wings that developed from discs of surgically pinched larvae (Pastor-Pareja et al., 2008; Kashio et al., 2014). Reducing JAK/STAT function in the posterior compartment by expressing an RNAi construct targeting *hop* caused a pronounced reduction in adult wing sizes developing from discs, in which pinching had been targeted to the posterior compartment as visualized by co-expression of GFP (Fig. S8B). In contrast, no reduction in size of the posterior compartment was observed for adult wings derived from undamaged control discs raised under the same conditions (not shown).

These data suggest that cellular responses to genetically or surgically induced damage critically rely on JAK/STAT activation to facilitate restoration of normal tissue homeostasis. Combined, our results strongly imply that a reduction in final tissue size upon JAK/STAT inhibition reflects an excessive loss of tissue due to cell death rather than a failure of the tissue to undergo compensatory proliferation.

JAK/STAT activity promotes efficient induction of compensatory responses

We wanted to investigate further if the observed reduction in adult wing sizes upon JAK/STAT inhibition is exclusively caused by a loss of tissue to cell death or if other regenerative processes may be disturbed. A process that contributes to successful tissue restoration is the induction of a dILP8-dependent developmental delay at the larval-pupal transition, which extends the time available for repair before metamorphosis (Colombani et al., 2012; Garelli et al., 2012). We found that interfering with JAK/STAT in *eiger*-expressing cells also caused a profound reduction in developmental delays induced by Eiger stimulation (Fig. 6C).

To understand if altered *Ilp8* expression caused this observation, we quantified expression of a *GFP*-reporter driven from the endogenous *Ilp8* locus (Garelli et al., 2012). We found that the reporter was strongly expressed in the pouch of Eiger-stimulated discs (Fig. S8C). In contrast, interfering with JAK/STAT by expression of *dome-RNAi* or $dome^{\Delta cyt}$ in *eiger*-expressing cells significantly reduced the area of GFP expression (Fig. 6D, Fig. S8D,E). This suggests that loss of *Ilp8* expression, caused by impaired JAK/STAT in JNK-signalling cells, underlies the observed failure to efficiently induce a developmental delay.

To test whether JAK/STAT signalling is sufficient to induce developmental delays, we expressed the JAK/STAT-ligands Upd1 or Upd2 in wild-type discs using *MS1096-GAL4*. However, no difference in pupariation timing between Upd-expressing and stage-matched wild-type larvae was observed (Fig. S8F). While a recent study links *Ilp8*-expression to JAK/STAT signalling (Katsuyama et al., 2015), our data implies that *Ilp8* is not a direct target gene of STAT92E. Instead, we suggest that cells that normally express *Ilp8* in response to JNK activation are more likely to die when JAK/STAT signalling is reduced, thereby preventing efficient expression of *Ilp8* and induction of a developmental delay. The failure to induce this important systemic response reduces the time available for repair and probably contributes to the decrease in recovered adult wing sizes that we observed upon genetic reduction of JAK/STAT signalling (Fig. 6B).

JAK/STAT regulates survival in a Ras^{V12}; $scrib^{2}$ tumour model

To understand if JAK/STAT generally acts as a survival-promoting pathway in the context of tissue stress, we revisited the role of JAK/STAT in established fly tumour models. Previous studies suggest that activation of JAK/STAT drives tumorous overgrowth in discs mutant for tumour suppressor genes, such as *scribbled* (*scrib*) or *Psc-Su(z)2* (Wu et al., 2010; Classen et al., 2009). *scrib* cells, similar to *eiger*-expressing cells, exhibit strong JNK activation, correlating with elevated transcription of Upd cytokines (Wu et al., 2010; Bunker et al., 2015; Leong et al., 2009; Brumby and Richardson, 2003). While *scrib* cells have a growth disadvantage if surrounded by wild-type cells, they efficiently cooperate with oncogenic Ras^{V12} to create invasive tumours in clonal assays

Development (2016) 143, 2907-2919 doi:10.1242/dev.132340

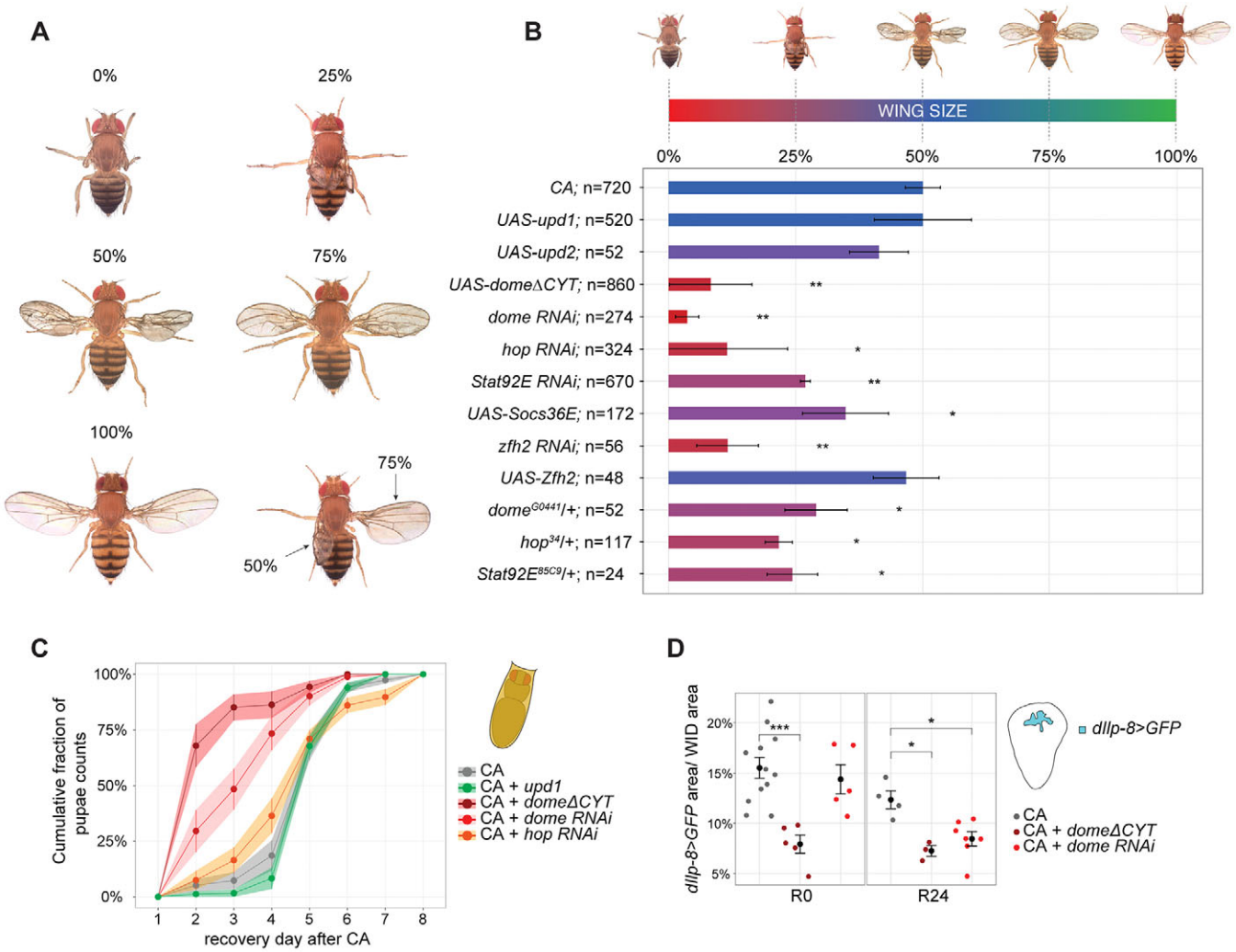

Fig. 6. JAK/STAT prevents excessive damage upon tissue stress. (A) Five adult wing size phenotypes were classified to score tissue damage after *eiger* expression at D7. (B) Average wing sizes developing from Eiger-stimulated disc (CA) or combined with *rn-GAL4*-mediated co-expression of UAS transgenes or in genetic backgrounds heterozygous for $dome^{G0441}$, hop^{34} or $Stat92E^{85C9}$. Graphs display mean±s.d. of average scores derived from ≥3 experiments. *t*-tests were performed to test for statistical significance (*P<0.05). *n*=number of wings scored. (C) Cumulative fraction of larvae undergoing larval-pupal transitions, which carry Eiger-stimulated discs (CA) (*n*=210) or were combined with *rn-GAL4*-mediated co-expression of *upd1* (*n*=213), $dome^{\Delta cyt}$ (*n*=201), *dome-RNAi* (*n*=196), or *hop-RNAi* (*n*=230). Graphs display mean±s.e.m. of average scores from ≥3 experiments. (D) Relative disc area expressing *llp8>GFP* after cell ablation (CA) (R0, *n*=12; R24, *n*=4 discs) and in discs combined with *rn-GAL4*-mediated co-expression of $dome^{\Delta cyt}$ (R0, *n*=5; R24, *n*=3 discs) or *dome-RNAi* (R0, *n*=5; R24, *n*=7 discs) in *eiger*-expressing cells. Graphs display mean±s.e.m. *U*-tests were performed to test for statistical significance (*P<0.05, **P<0.01, ***P<0.001).

(Brumby and Richardson, 2003; Wu et al., 2010). Larvae carrying MARCM-induced Ras^{V12}; $scrib^{2}$ clones fail to pupariate (Fig. 7M), suggesting that *Ilp8* activation correlates with tumour load (Garelli et al., 2012). We found that Ras^{V12}; $scrib^{2}$ clones covered about 47% of eye antennal discs, compared with 19% for wild-type clones (Fig. 7A,B,D). When we probed Ras^{V12}; $scrib^{2}$ clones for activated Dcp-1, we did not observe any difference in apoptotic patterns compared with wild-type tissue (Fig. 7F,G).

When we completely removed JAK/STAT function in Ras^{V12}; $scrib^{2}$ clones by homozygosity for a $Stat92E^{85C9}$ allele, Ras^{V12}; $scrib^{2}$ clone size was reduced from 47% to 28% of the eye disc area (Fig. 7B-D). Comparison of cell division rates within Ras^{V12}; $scrib^{2}$ and Ras^{V12}; $scrib^{2}$, $Stat92E^{85C9}$ clones did not reveal any significant changes upon loss of JAK/STAT function (Fig. 7B′,C′,E). However, in contrast to Ras^{V12}; $scrib^{2}$ clones, Ras^{V12}; $scrib^{2}$, $Stat92E^{85C9}$ clones displayed a 4.3-fold increase in areas of Dcp-1 activation (Fig. 7G,H,I), suggesting that increased cell death of *Stat92E* mutant cells underlies the smaller sizes of Ras^{V12}; $scrib^{2}$, $Stat92E^{85C9}$ clones (Fig. 7A-D). The reduction in Ras^{V12}; $scrib^{2}$, $Stat92E^{85C9}$ clone size reduced total tumour load and allowed a significant proportion of host larvae to progress to pupal stages (Fig. 7M).

Strikingly, Ras^{V12}; $scrib^{2}$ clones displayed ectopic activation of Zfh2 (Fig. 7J,K) but not of Zfh1 (not shown), indicating activation of a JNK-JAK/STAT-Zfh2 stress module by neoplastic transformation. Importantly, ectopic expression of Zfh2 was completely abolished within Ras^{V12}; $scrib^{2}$, $Stat92E^{85C9}$ clones (Fig. 7L). These results support the notion that Zfh2 expression is regulated by JAK/STAT in multiple contexts of cellular stress and that stress-dependent Zfh2 activation in imaginal discs directly correlates with cell survival.

Altogether, our results support a model in which cellular stress caused by genetic cell ablation, physical wounding or tumorous growth drives activation of JAK/STAT to promote survival of

Development (2016) 143, 2907-2919 doi:10.1242/dev.132340

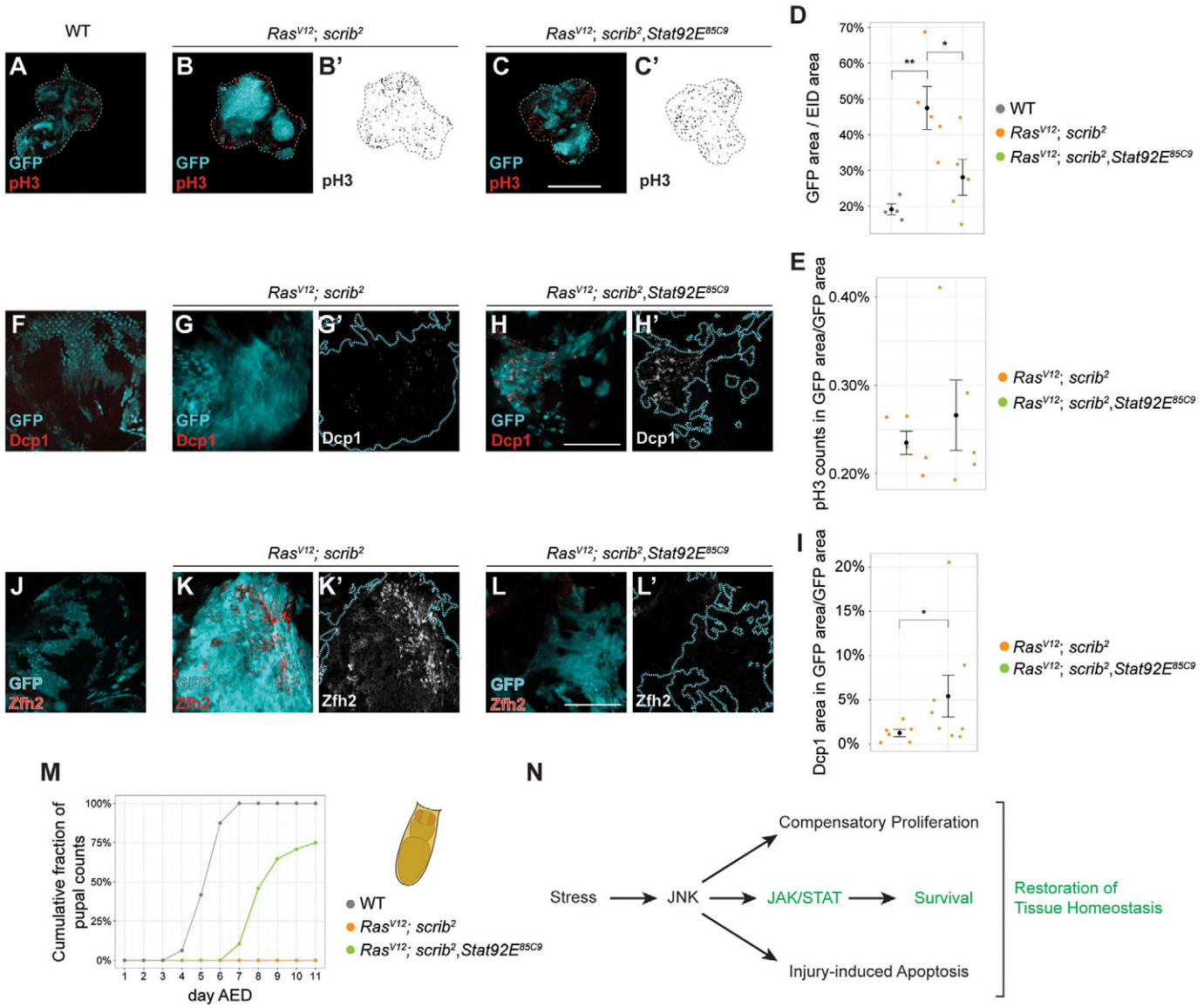

Fig. 7. JAK/STAT regulates survival in a *Ras^{V12}; scrib^{2}* tumour model. (A-C) Eye imaginal discs carrying neutral (A), *Ras^{V12}; scrib^{2}* (B,B′) or *Ras^{V12}; scrib^{2}, Stat92E^{85C9}* (C,C′). GFP-marked MARCM clones (cyan in A-C) stained for pH3 (B′,C′, red in A-C). (D) Area occupied by neutral (n=4), *Ras^{V12}; scrib^{2}* (n=5) or *Ras^{V12}; scrib^{2}, Stat92E^{85C9}* (n=5) clones, normalized to total eye imaginal disc (EID) area. (E) pH3-events in *Ras^{V12}; scrib^{2}* (n=5) or *Ras^{V12}; scrib^{2}, Stat92E^{85C9}* (n=5) clones per eye disc normalized to total clone area per disc. (F-H) Eye discs carrying neutral (F), *Ras^{V12}; scrib^{2}* (G,G′) or *Ras^{V12}; scrib^{2}, Stat92E^{85C9}* (H,H′) clones (cyan in F-H) stained for Dcp-1 (G′,H′, red in F-H). Clone borders indicated by outline in G′,H′. (I) Dcp-1-positive area within *Ras^{V12}; scrib^{2}* (n=6) or *Ras^{V12}; scrib^{2}, Stat92E^{85C9}* (n=8) clones normalized to total clone area per disc. (J-L) Eye discs carrying neutral (J), *Ras^{V12}; scrib^{2}* (K,K′) or *Ras^{V12}; scrib^{2}, Stat92E^{85C9}* (L,L′) clones (cyan in J-L) stained for Zfh2 (K′,L′, red in J-L). (M) Cumulative fraction of larvae undergoing larval-pupal transitions carrying *Ras^{V12}; scrib^{2}* or *Ras^{V12}; scrib^{2}, Stat92E^{85C9}* clones. (N) Cells activating JNK in response to stress induce compensatory proliferation as well as injury-induced apoptosis. JAK/STAT suppresses apoptosis, thereby limiting the extent of tissue damage and promoting compensatory responses, such as induction of development delays. Graphs display mean±s.e.m. *U*-tests were performed to test for statistical significance (*P<0.05, **P<0.01, ***P<0.001). Scale bars: 100 µm.

JNK-signalling cells. Activation of JAK/STAT signalling thereby facilitates the induction and execution of local and systemic compensatory responses, rather than promoting compensatory cell proliferation directly (Fig. 7N).

DISCUSSION

JNK activation during tissue stress drives elimination of damaged cells by apoptosis (Bogoyevitch et al., 2010; Chen, 2012; Shlevkov and Morata, 2012; Luo et al., 2007; Moreno et al., 2002) and compensatory proliferation necessary to replace lost tissues (Bosch et al., 2005; Bergantinos et al., 2010; Mattila et al., 2005; Ryoo et al., 2004; Sun and Irvine, 2011). Our work provides an answer to the central question of how these Janus-faced responses can be balanced by JNK. We show that in contrast to prevalent models, JAK/STAT signalling downstream of JNK does not promote compensatory proliferation, but instead supports cell survival and thereby contributes to tissue growth (Fig. 7N). The decision between JAK/STAT-dependent survival and JNK-induced apoptosis may depend on a relative cellular ratio between JAK/STAT and JNK signalling, which is determined by the position of cells within respective signalling gradients (Fig. S9B,B′). As a consequence of its pro-survival function, JAK/STAT indirectly supports regenerative growth by allowing JNK to initiate dILP8-dependent developmental delays and,

Development (2016) 143, 2907-2919 doi:10.1242/dev.132340

possibly, by facilitating Hippo/Yorkie-driven proliferation (Sun and Irvine, 2014). In fact, JNK-dependent Yorkie activation (Sun and Irvine, 2011) may occur independent of Jun/Fos-mediated transcription (Sun and Irvine, 2013), therefore JAK/STAT and Zfh2-dependent repression of *kay/fos* could suppress induction of JNK-dependent apoptosis without suppressing activation of Yorkie and thus of Hippo/Yorkie-driven compensatory proliferation. Hippo/Yorkie signalling, in turn, may sustain activation of *unpaired* and JAK/STAT signalling (Staley and Irvine, 2010; Bunker et al., 2015; Sarikaya and Extavour, 2015) even if JNK signalling is low. This signalling crosstalk would facilitate the stabilisation of a wound-proximal tissue domain supporting compensatory survival and proliferation.

Our new interpretation of JAK/STAT in promoting cell survival in response to tissue damage and in tumours can be reconciled with previous studies: JAK/STAT mutations frequently reduced tissue size. This was interpreted as a reduction in growth (Classen et al., 2009; Wu et al., 2010; Mukherjee et al., 2005; Amoyel et al., 2014), but we suggest that it is a consequence of excessive cell death. Similarly, Upd overexpression has been previously reported to drive cell proliferation (Bach et al., 2003; Classen et al., 2009; Tsai and Sun, 2004). However, continuous overexpression of Upd can also induce apoptosis (not shown) and, thus potentially also sustained JNK-dependent compensatory proliferation, driving tissue growth. So far, only isolated studies have implicated JAK/STAT in cell survival (Betz et al., 2008; Hasan et al., 2015; Guarner et al., 2014; Ohayon et al., 2009). For example, the apoptosis inhibitor *IAP* has been suggested to be a positively regulated target of Stat92E, protecting cells from apoptosis (Betz et al., 2008; Hasan et al., 2015). We identify the JAK/STAT effector Zfh2 as a potential repressor of *kay* and *hid* activity – a molecular pathway expected to restrain excessive JNK-activity and induction of apoptosis (Fig. S9A). Similarly, Dpp/TGFβ-dependent repression of *rpr* by Schnurri has been reported to prevent JNK-mediated apoptosis. Curiously, this occurs in contexts where JNK function is required to mediate cell shape remodelling during development (Beira et al., 2014) and therefore bears conceptual similarities to a model where JAK/STAT-dependent repression of *kay* and *hid* prevents JNK-mediated apoptosis but not Hippo/Yorkie-dependent compensatory proliferation. Our work does not address whether JAK/STAT only promotes survival during stress or if this also occurs during development. Cells carrying JAK/STAT mutations are eliminated from developing wing discs (Rodrigues et al., 2012) by cell competition. However, in the light of recent studies, which implicate JNK signalling in competitive cell elimination (Kolahgar et al., 2015), more studies are clearly needed to dissect the functional contribution of stress signals in this context. Combined, these studies and our work suggest that JNK-dependent apoptosis can be counteracted by multiple molecular pathways impinging on anti- and pro-apoptotic genes.

While the role of mammalian IL-6/STAT3 in regeneration needs to be further investigated, much evidence points to JNK and JAK/STAT pathways as crucial mediators of compensatory responses and tumorigenesis in mammalian tissues (Chen, 2012). A previous report suggests that JAK/STAT activation during mouse liver regeneration potentially confers a cell-protective function, similarly facilitating initiation of compensatory responses, rather then directly promoting cell proliferation (Wuestefeld et al., 2003). Therefore, the dominant pro-survival function of JAK/STAT in response to tissue stress, which we find to be essential for successful restoration of tissue homeostasis, appears highly relevant to human contexts of cellular stress in physiological or pathological conditions.

MATERIALS AND METHODS

Drosophila stocks

For a detailed list of genotypes used in all experiments and shown in figures, refer to Table S1.

Temporal and spatial control of *eiger* expression

Fly crosses were carried out as described in supplementary Materials and Methods and *eiger* expression was induced as described in Smith-Bolton et al. (2009) and Fig. S1.

Immunohistochemistry

Larval cuticles were fixed in 4% PFA/PBS for 15 min at room temperature. Washing steps were performed in 0.1% Triton X-100/PBS (PBT), blocking in 5% NGS/PBT. Tissue samples were incubated in the following primary antibodies overnight at 4°C: mouse anti-Nub (1:100, S. Cohen, University of Copenhagen), rabbit anti-GFP (1:1000, Immunokontakt, cat. no. 210-PS-1GFP), mouse anti-H3S10p (1:2000, Abcam, cat. no. ab14955), rabbit anti-cCasp-3 (1:500, Cell Signaling, cat. no. 9661), rabbit anti-Dcp1 (1:500, Cell Signaling, cat. no. 9578), rabbit anti-β-Gal (1:500, Cappel, cat. no. 559762), rat anti-Zfh1 (1:500, R. Lehmann, NYU School of Medicine), rat anti-Zfh2 (1:300, C. Doe, HHMI/Institute of Molecular Biology). Secondary antibodies (Molecular Probes), DAPI and phalloidin-TRITC (Sigma) were applied and samples were incubated for 2 h at room temperature.

Flow cytometry and BrdU labelling

Flow cytometry of wing imaginal disc cells and labelling of fixed cuticle tissue with BrdU was carried out using standard techniques as described in supplementary Materials and Methods.

Real-time qPCR

RNA was extracted from ∼80 wing discs using Qiagen RNAlater and RNeasy protocols. cDNA libraries were prepared using standard protocols, including Ambion TurboDNase and Invitrogen Superscript III kits. qPCR was performed using Fast SYBR Green (Applied Biosystems) on a CFX-96 Real-Time machine (Bio-Rad). Data were analysed using the $\Delta\Delta C_t$ method and normalized to at least two housekeeping genes (Table S2).

Transcription factor binding site prediction

Bioinformatic analysis for potential transcription factor binding sites was performed using the program Clover (cis-element over-representation) (Frith et al., 2004) in combination with position-weighted matrices (PWM) obtained from the JASPAR collection (Mathelier et al., 2014) as detailed in supplementary Materials and Methods.

Adult wing size analysis

Wing size index (Ws) was calculated as the mean of five different wing phenotypes (w) (Fig. 5A) weighted with the frequencies at which they occurred (f) ($Ws=\Sigma w_i \times f_i/\Sigma f_i$). Samples were compared in a paired manner to control wings from the same experimental replicate (Wilcoxon signed rank test, $\alpha=0.05$, $n\geq3$ sample populations).

Acknowledgements

We thank R. Smith-Bolton, D. Bohmann, E. Bach, G. Halder, S. Cohen, R. Lehmann, C. Doe, E. Sanchez-Herrero, F. Diaz-Benjumea, N. Gompel and H. Leonhardt for sharing reagents and resources. We thank Bloomington and VDRC for fly stocks, and DSHB for antibodies. We thank the LSM, IMPRS-LS and IRTG-SFB1064 graduate schools for supporting our students.

Competing interests

The authors declare no competing or financial interests.

Author contributions

Designed the experiments: M.L.F., A.-K.C. Performed the experiments: M.L.F., M.S., A.C., A.K., I.G., A.-K.C. Data analysis: M.L.F., M.S., A.C., A.-K.C. Wrote the paper: M.L.F., A.-K.C.

Development (2016) 143, 2907-2919 doi:10.1242/dev.132340

Funding
This research was funded by the Deutsche Forschungsgemeinschaft [CL490-1 to A.-K.C.]

Supplementary information
Supplementary information available online at
http://dev.biologists.org/lookup/doi/10.1242/dev.132340.supplemental

References

Amoyel, M., Anderson, A. M. and Bach, E. A. (2014). JAK/STAT pathway dysregulation in tumors: a Drosophila perspective. *Semin. Cell Dev. Biol.* **28**, 96-103.
Andersen, D. S., Colombani, J., Palmerini, V., Chakrabandhu, K., Boone, E., Röthlisberger, M., Toggweiler, J., Basler, K., Mapelli, M., Hueber, A.-O. et al. (2015). The Drosophila TNF receptor Grindelwald couples loss of cell polarity and neoplastic growth. *Nature* **522**, 482-486.
Arbouzova, N. I. and Zeidler, M. P. (2006). JAK/STAT signalling in Drosophila: insights into conserved regulatory and cellular functions. *Development* **133**, 2605-2616.
Ayala-Camargo, A., Ekas, L. A., Flaherty, M. S., Baeg, G. -H. and Bach, E. A. (2007). The JAK/STAT pathway regulates proximo-distal patterning in Drosophila. *Dev. Dyn.* **236**, 2721-2730.
Ayala-Camargo, A., Anderson, A. M., Amoyel, M., Rodrigues, A. B., Flaherty, M. S. and Bach, E. A. (2013). JAK/STAT signaling is required for hinge growth and patterning in the Drosophila wing disc. *Dev. Biol.* **382**, 413-426.
Bach, E. A., Vincent, S., Zeidler, M. P. and Perrimon, N. (2003). A sensitized genetic screen to identify novel regulators and components of the Drosophila janus kinase/signal transducer and activator of transcription pathway. *Genetics* **165**, 1149-1166.
Bach, E. A., Ekas, L. A., Ayala-Camargo, A., Flaherty, M. S., Lee, H., Perrimon, N. and Baeg, G.-H. (2007). GFP reporters detect the activation of the Drosophila JAK/STAT pathway in vivo. *Gene Expr. Patterns* **7**, 323-331.
Bando, T., Ishimaru, Y., Kida, T., Hamada, Y., Matsuoka, Y., Nakamura, T., Ohuchi, H., Noji, S. and Mito, T. (2013). Analysis of RNA-Seq data reveals involvement of JAK/STAT signalling during leg regeneration in the cricket Gryllus bimaculatus. *Development* **140**, 959-964.
Beira, J. V., Springhorn, A., Gunther, S., Hufnagel, L., Pyrowolakis, G. and Vincent, J. -P. (2014). The Dpp/TGFbeta-dependent corepressor Schnurri protects epithelial cells from JNK-induced apoptosis in drosophila embryos. *Dev. Cell* **31**, 240-247.
Bergantinos, C., Corominas, M. and Serras, F. (2010). Cell death-induced regeneration in wing imaginal discs requires JNK signalling. *Development* **137**, 1169-1179.
Betz, A., Ryoo, H. D., Steller, H. and Darnell, J. E., Jr. (2008). STAT92E is a positive regulator of Drosophila inhibitor of apoptosis 1 (DIAP/1) and protects against radiation-induced apoptosis. *Proc. Natl. Acad. Sci. USA* **105**, 13805-13810.
Bogoyevitch, M. A., Ngoei, K. R. W., Zhao, T. T., Yeap, Y. Y. C. and Ng, D. C. H. (2010). c-Jun N-terminal kinase (JNK) signaling: recent advances and challenges. *Biochim. Biophys. Acta* **1804**, 463-475.
Bosch, M., Serras, F., Martín-Blanco, E. and Baguñà, J. (2005). JNK signaling pathway required for wound healing in regenerating Drosophila wing imaginal discs. *Dev. Biol.* **280**, 73-86.
Bosch, M., Bagun, J. and Serras, F. (2008). Origin and proliferation of blastema cells during regeneration of Drosophila wing imaginal discs. *Int. J. Dev. Biol.* **52**, 1043-1050.
Bray, N., Dubchak, I. and Pachter, L. (2003). AVID: a global alignment program. *Genome Res.* **13**, 97-102.
Brumby, A. M. and Richardson, H. E. (2003). scribble mutants cooperate with oncogenic Ras or Notch to cause neoplastic overgrowth in Drosophila. *EMBO J.* **22**, 5769-5779.
Bryant, P. J. (1975). Regeneration and duplication in imaginal discs. *Ciba Found. Symp.* **0**, 71-93.
Bunker, B. D., Nellimoottil, T. T., Boileau, R. M., Classen, A. K. and Bilder, D. (2015). The transcriptional response to tumorigenic polarity loss in Drosophila. *eLife* **4**, e03189.
Chatterjee, N. and Bohmann, D. (2012). A versatile PhiC31 based reporter system for measuring AP-1 and Nrf2 signaling in Drosophila and in tissue culture. *PLoS ONE* **7**, e34063.
Chen, F. (2012). JNK-induced apoptosis, compensatory growth, and cancer stem cells. *Cancer Res.* **72**, 379-386.
Classen, A.-K., Bunker, B. D., Harvey, K. F., Vaccari, T. and Bilder, D. (2009). A tumor suppressor activity of Drosophila Polycomb genes mediated by JAK-STAT signaling. *Nat. Genet.* **41**, 1150-1155.
Colombani, J., Andersen, D. S. and Leopold, P. (2012). Secreted peptide Dilp8 coordinates Drosophila tissue growth with developmental timing. *Science* **336**, 582-585.
Cressman, D. E., Greenbaum, L. E., Deangelis, R. A., Ciliberto, G., Furth, E. E., Poli, V. and Taub, R. (1996). Liver failure and defective hepatocyte regeneration in interleukin-6-deficient mice. *Science* **274**, 1379-1383.
Davie, K., Jacobs, J., Atkins, M., Potier, D., Christiaens, V., Halder, G. and Aerts, S. (2015). Discovery of transcription factors and regulatory regions driving in vivo tumor development by ATAC-seq and FAIRE-seq open chromatin profiling. *PLoS Genet.* **11**, e1004994.
Eferl, R. and Wagner, E. F. (2003). AP-1: a double-edged sword in tumorigenesis. *Nat. Rev. Cancer* **3**, 859-868.
Evans, C. J., Olson, J. M., Ngo, K. T., Kim, E., Lee, N. E., Kuoy, E., Patananan, A. N., Sitz, D., Tran, P., Do, M.-T. et al. (2009). G-TRACE: rapid Gal4-based cell lineage analysis in Drosophila. *Nat. Methods* **6**, 603-605.
Fan, Y. and Bergmann, A. (2008). Distinct mechanisms of apoptosis-induced compensatory proliferation in proliferating and differentiating tissues in the Drosophila eye. *Dev. Cell* **14**, 399-410.
Flaherty, M. S., Salis, P., Evans, C. J., Ekas, L. A., Marouf, A., Zavadil, J., Banerjee, U. and Bach, E. A. (2010). chinmo is a functional effector of the JAK/STAT pathway that regulates eye development, tumor formation, and stem cell self-renewal in Drosophila. *Dev. Cell* **18**, 556-568.
Frazer, K. A., Pachter, L., Poliakov, A., Rubin, E. M. and Dubchak, I. (2004). VISTA: computational tools for comparative genomics. *Nucleic Acids Res.* **32**, W273-W279.
Frith, M. C., Fu, Y., Yu, L., Chen, J.-F., Hansen, U. and Weng, Z. (2004). Detection of functional DNA motifs via statistical over-representation. *Nucleic Acids Res.* **32**, 1372-1381.
Fulda, S., Gorman, A. M., Hori, O. and Samali, A. (2010). Cellular stress responses: cell survival and cell death. *Int. J. Cell Biol.* **2010**, 214074.
Garelli, A., Gontijo, A. M., Miguela, V., Caparros, E. and Dominguez, M. (2012). Imaginal discs secrete insulin-like peptide 8 to mediate plasticity of growth and maturation. *Science* **336**, 579-582.
Gregory, L., Came, P. J. and Brown, S. (2008). Stem cell regulation by JAK/STAT signaling in Drosophila. *Semin. Cell Dev. Biol.* **19**, 407-413.
Grusche, F. A., Degoutin, J. L., Richardson, H. E. and Harvey, K. F. (2011). The Salvador/Warts/Hippo pathway controls regenerative tissue growth in Drosophila melanogaster. *Dev. Biol.* **350**, 255-266.
Guarner, A., Manjón, C., Edwards, K., Steller, H., Suzanne, M. and Sánchez-Herrero, E. (2014). The zinc finger homeodomain-2 gene of Drosophila controls Notch targets and regulates apoptosis in the tarsal segments. *Dev. Biol.* **385**, 350-365.
Hasan, S., Hétié, P. and Matunis, E. L. (2015). Niche signaling promotes stem cell survival in the Drosophila testis via the JAK–STAT target DIAP1. *Dev. Biol.* **404**, 27-39.
Haynie, J. L. and Bryant, P. J. (1976). Intercalary regeneration in imaginal wing disk of Drosophila melanogaster. *Nature* **259**, 659-662.
Herrera, S. C. and Morata, G. (2014). Transgressions of compartment boundaries and cell reprogramming during regeneration in Drosophila. *eLife* **3**, e01831.
Herrera, S. C., Martín, R. and Morata, G. (2013). Tissue homeostasis in the wing disc of Drosophila melanogaster: immediate response to massive damage during development. *PLoS Genet.* **9**, e1003446.
Herz, H. -M., Chen, Z., Scherr, H., Lackey, M., Bolduc, C. and Bergmann, A. (2006). vps25 mosaics display non-autonomous cell survival and overgrowth, and autonomous apoptosis. *Development* **133**, 1871-1880.
Huh, J. R., Guo, M. and Hay, B. A. (2004). Compensatory proliferation induced by cell death in the Drosophila wing disc requires activity of the apical cell death caspase Dronc in a nonapoptotic role. *Curr. Biol.* **14**, 1262-1266.
Igaki, T. (2009). Correcting developmental errors by apoptosis: lessons from Drosophila JNK signaling. *Apoptosis* **14**, 1021-1028.
Igaki, T. and Miura, M. (2014). The Drosophila TNF ortholog Eiger: emerging physiological roles and evolution of the TNF system. *Semin. Immunol.* **26**, 267-274.
Igaki, T., Kanda, H., Yamamoto-Goto, Y., Kanuka, H., Kuranaga, E., Aigaki, T. and Miura, M. (2002). Eiger, a TNF superfamily ligand that triggers the Drosophila JNK pathway. *EMBO J.* **21**, 3009-3018.
Jiang, H., Patel, P. H., Kohlmaier, A., Grenley, M. O., Mcewen, D. G. and Edgar, B. A. (2009). Cytokine/Jak/Stat signaling mediates regeneration and homeostasis in the Drosophila midgut. *Cell* **137**, 1343-1355.
Johnstone, K., Wells, R. E., Strutt, D. and Zeidler, M. P. (2013). Localised JAK/STAT pathway activation is required for Drosophila wing hinge development. *PLoS ONE* **8**, e65076.
Kashio, S., Obata, F. and Miura, M. (2014). Interplay of cell proliferation and cell death in Drosophila tissue regeneration. *Dev. Growth Differ.* **56**, 368-375.
Katsuyama, T., Comoglio, F., Seimiya, M., Cabuy, E. and Paro, R. (2015). During Drosophila disc regeneration, JAK/STAT coordinates cell proliferation with Dilp8-mediated developmental delay. *Proc. Natl. Acad. Sci. USA* **112**, E2327-E2336.
Kolahgar, G., Suijkerbuijk, S. J. E., Kucinski, I., Poirier, E. Z., Mansour, S., Simons, B. D. and Piddini, E. (2015). Cell competition modifies adult stem cell and tissue population dynamics in a JAK-STAT-dependent manner. *Dev. Cell* **34**, 297-309.
Kondo, S., Senoo-Matsuda, N., Hiromi, Y. and Miura, M. (2006). DRONC coordinates cell death and compensatory proliferation. *Mol. Cell. Biol.* **26**, 7258-7268.

Leatherman, J. L. and Dinardo, S. (2008). Zfh-1 controls somatic stem cell self-renewal in the Drosophila testis and nonautonomously influences germline stem cell self-renewal. *Cell Stem Cell* **3**, 44-54.
Lee, N., Maurange, C., Ringrose, L. and Paro, R. (2005). Suppression of Polycomb group proteins by JNK signalling induces transdetermination in Drosophila imaginal discs. *Nature* **438**, 234-237.
Leong, G. R., Goulding, K. R., Amin, N., Richardson, H. E. and Brumby, A. M. (2009). Scribble mutants promote aPKC and JNK-dependent epithelial neoplasia independently of Crumbs. *BMC Biol.* **7**, 62.
Li, W., Liang, X., Kellendonk, C., Poli, V. and Taub, R. (2002). STAT3 contributes to the mitogenic response of hepatocytes during liver regeneration. *J. Biol. Chem.* **277**, 28411-28417.
Lin, G., Xu, N. and Xi, R. (2009). Paracrine unpaired signaling through the JAK/STAT pathway controls self-renewal and lineage differentiation of drosophila intestinal stem cells. *J. Mol. Cell Biol* **2**, 37-49.
Luo, X., Puig, O., Hyun, J., Bohmann, D. and Jasper, H. (2007). Foxo and Fos regulate the decision between cell death and survival in response to UV irradiation. *EMBO J.* **26**, 380-390.
Martin, F. A., Perez-Garijo, A. and Morata, G. (2009). Apoptosis in Drosophila: compensatory proliferation and undead cells. *Int. J. Dev. Biol.* **53**, 1341-1347.
Mathelier, A., Zhao, X., Zhang, A. W., Parcy, F., Worsley-Hunt, R., Arenillas, D. J., Buchman, S., Chen, C. Y., Chou, A., Ienasescu, H. et al. (2014). JASPAR 2014: An extensively expanded and updated open-access database of transcription factor binding profiles. *Nucleic Acids Res.* **42**, D142-D147.
Mattila, J., Omelyanchuk, L., Kyttala, S., Turunen, H. and Nokkala, S. (2005). Role of Jun N-terminal Kinase (JNK) signaling in the wound healing and regeneration of a Drosophila melanogaster wing imaginal disc. *Int. J. Dev. Biol.* **49**, 391-399.
Moberg, K. H., Schelble, S., Burdick, S. K. and Hariharan, I. K. (2005). Mutations in erupted, the Drosophila ortholog of mammalian tumor susceptibility gene 101, elicit non-cell-autonomous overgrowth. *Dev. Cell* **9**, 699-710.
Morata, G., Shlevkov, E. and Pérez-Garijo, A. (2011). Mitogenic signaling from apoptotic cells in Drosophila. *Dev. Growth Differ.* **53**, 168-176.
Moreno, E., Yan, M. and Basler, K. (2002). Evolution of TNF signaling mechanisms: JNK-dependent apoptosis triggered by Eiger, the Drosophila homolog of the TNF superfamily. *Curr. Biol.* **12**, 1263-1268.
Mukherjee, T., Hombría, J. C.-G. and Zeidler, M. P. (2005). Opposing roles for Drosophila JAK/STAT signalling during cellular proliferation. *Oncogene* **24**, 2503-2511.
Myllymäki, H. and Rämet, M. (2014). JAK/STAT pathway in Drosophila immunity. *Scand. J. Immunol.* **79**, 377-385.
Ohayon, D., Pattyn, A., Venteo, S., Valmier, J., Carroll, P. and Garces, A. (2009). Zfh1 promotes survival of a peripheral glia subtype by antagonizing a Jun N-terminal kinase-dependent apoptotic pathway. *EMBO J.* **28**, 3228-3243.
Ohlstein, B. and Spradling, A. (2006). The adult Drosophila posterior midgut is maintained by pluripotent stem cells. *Nature* **439**, 470-474.
Osman, D., Buchon, N., Chakrabarti, S., Huang, Y. -T., Su, W.-C., Poidevin, M., Tsai, Y.-C. and Lemaitre, B. (2013). Autocrine and paracrine unpaired signaling regulate intestinal stem cell maintenance and division. *J. Cell Sci.* **125**, 5944-5949.
Pahlavan, P. S., Feldmann, R. E., Jr., Zavos, C. and Kountouras, J. (2006). Prometheus' challenge: molecular, cellular and systemic aspects of liver regeneration. *J. Surg. Res.* **134**, 238-251.
Pastor-Pareja, J. C. and Xu, T. (2013). Dissecting social cell biology and tumors using Drosophila genetics. *Annu. Rev. Genet.* **47**, 51-74.
Pastor-Pareja, J. C., Wu, M. and Xu, T. (2008). An innate immune response of blood cells to tumors and tissue damage in Drosophila. *Dis. Model. Mech.* **1**, 144-154; discussion 153.
Perea, D., Molohon, K., Edwards, K. and Díaz-Benjumea, F. J. (2013). Multiple roles of the gene zinc finger homeodomain-2 in the development of the Drosophila wing. *Mech. Dev.* **130**, 467-481.
Pérez-Garijo, A., Martín, F. A. and Morata, G. (2004). Caspase inhibition during apoptosis causes abnormal signalling and developmental aberrations in Drosophila. *Development* **131**, 5591-5598.
Perez-Garijo, A., Shlevkov, E. and Morata, G. (2009). The role of Dpp and Wg in compensatory proliferation and in the formation of hyperplastic overgrowths caused by apoptotic cells in the Drosophila wing disc. *Development* **136**, 1169-1177.
Pérez-Garijo, A., Fuchs, Y. and Steller, H. (2013). Apoptotic cells can induce non-autonomous apoptosis through the TNF pathway. *eLife* **2**, e01004.
Postigo, A. A. and Dean, D. C. (1999). Independent repressor domains in ZEB regulate muscle and T-cell differentiation. *Mol. Cell. Biol.* **19**, 7961-7971.
Postigo, A. A., Ward, E., Skeath, J. B. and Dean, D. C. (1999). zfh-1, the Drosophila homologue of ZEB, is a transcriptional repressor that regulates somatic myogenesis. *Mol. Cell. Biol.* **19**, 7255-7263.
Rämet, M., Lanot, R., Zachary, D. and Manfruelli, P. (2002). JNK signaling pathway is required for efficient wound healing in Drosophila. *Dev. Biol.* **241**, 145-156.
Razzell, W., Wood, W. and Martin, P. (2011). Swatting flies: modelling wound healing and inflammation in Drosophila. *Dis. Model. Mech.* **4**, 569-574.
Repiso, A., Bergantinos, C. and Serras, F. (2013). Cell fate respecification and cell division orientation drive intercalary regeneration in Drosophila wing discs. *Development* **140**, 3541-3551.
Ríos-Barrera, L. D. and Riesgo-Escovar, J. R. (2013). Regulating cell morphogenesis: the Drosophila Jun N-terminal kinase pathway. *Genesis* **51**, 147-162.
Rodrigues, A. B., Zoranovic, T., Ayala-Camargo, A., Grewal, S., Reyes-Robles, T., Krasny, M., Wu, D. C., Johnston, L. A. and Bach, E. A. (2012). Activated STAT regulates growth and induces competitive interactions independently of Myc, Yorkie, Wingless and ribosome biogenesis. *Development* **139**, 4051-4061.
Ryoo, H. D., Gorenc, T. and Steller, H. (2004). Apoptotic cells can induce compensatory cell proliferation through the JNK and the Wingless signaling pathways. *Dev. Cell* **7**, 491-501.
Santabárbara-Ruiz, P., López-Santillán, M., Martínez-Rodríguez, I., Binagui-Casas, A., Pérez, L., Milán, M., Corominas, M. and Serras, F. (2015). ROS-Induced JNK and p38 signaling is required for unpaired cytokine activation during Drosophila regeneration. *PLoS Genet.* **11**, e1005595.
Sarikaya, D. P. and Extavour, C. G. (2015). The Hippo pathway regulates homeostatic growth of stem cell niche precursors in the Drosophila ovary. *PLoS Genet.* **11**, e1004962.
Schroeder, M. C., Chen, C.-L., Gajewski, K. and Halder, G. (2013). A non-cell-autonomous tumor suppressor role for Stat in eliminating oncogenic scribble cells. *Oncogene* **32**, 4471-4479.
Schuster, K. J. and Smith-Bolton, R. K. (2015). Taranis protects regenerating tissue from fate changes induced by the wound response in Drosophila. *Dev. Cell* **34**, 119-128.
Shlevkov, E. and Morata, G. (2012). A dp53/JNK-dependant feedback amplification loop is essential for the apoptotic response to stress in Drosophila. *Cell Death Differ.* **19**, 451-460.
Smith-Bolton, R. K., Worley, M. I., Kanda, H. and Hariharan, I. K. (2009). Regenerative growth in Drosophila imaginal discs is regulated by Wingless and Myc. *Dev. Cell* **16**, 797-809.
Staley, B. K. and Irvine, K. D. (2010). Warts and Yorkie mediate intestinal regeneration by influencing stem cell proliferation. *Curr. Biol.* **20**, 1580-1587.
Sun, G. and Irvine, K. D. (2011). Regulation of Hippo signaling by Jun kinase signaling during compensatory cell proliferation and regeneration, and in neoplastic tumors. *Dev. Biol.* **350**, 139-151.
Sun, G. and Irvine, K. D. (2013). Ajuba family proteins link JNK to Hippo signaling. *Sci. Signal.* **6**, ra81.
Sun, G. and Irvine, K. D. (2014). Control of growth during regeneration. *Curr. Top. Dev. Biol.* **108**, 95-120.
Sustar, A., Bonvin, M., Schubiger, M. and Schubiger, G. (2011). Drosophila twin spot clones reveal cell division dynamics in regenerating imaginal discs. *Dev. Biol.* **356**, 576-587.
Tsai, Y.-C. and Sun, Y. H. (2004). Long-range effect of upd, a ligand for Jak/STAT pathway, on cell cycle in Drosophila eye development. *Genesis* **39**, 141-153.
Uhlirova, M., Jasper, H. and Bohmann, D. (2005). Non-cell-autonomous induction of tissue overgrowth by JNK/Ras cooperation in a Drosophila tumor model. *Proc. Natl. Acad. Sci. USA* **102**, 13123-13128.
Vaccari, T. and Bilder, D. (2005). The Drosophila tumor suppressor vps25 prevents nonautonomous overproliferation by regulating notch trafficking. *Dev. Cell* **9**, 687-698.
Wells, B. S., Yoshida, E. and Johnston, L. A. (2006). Compensatory proliferation in Drosophila imaginal discs requires Dronc-dependent p53 activity. *Curr. Biol.* **16**, 1606-1615.
Wu, M., Pastor-Pareja, J. C. and Xu, T. (2010). Interaction between Ras(V12) and scribbled clones induces tumour growth and invasion. *Nature* **463**, 545-548.
Wuestefeld, T., Klein, C., Streetz, K. L., Betz, U., Lauber, J., Buer, J., Manns, M. P., Muller, W. and Trautwein, C. (2003). Interleukin-6/glycoprotein 130-dependent pathways are protective during liver regeneration. *J. Biol. Chem.* **278**, 11281-11288.
Yamada, Y., Kirillova, I., Peschon, J. J. and Fausto, N. (1997). Initiation of liver growth by tumor necrosis factor: deficient liver regeneration in mice lacking type I tumor necrosis factor receptor. *Proc. Natl. Acad. Sci. USA* **94**, 1441-1446.
Zhao, X. -F., Wan, J., Powell, C., Ramachandran, R., Myers, M. G., Jr. and Goldman, D. (2014). Leptin and IL-6 family cytokines synergize to stimulate Muller glia reprogramming and retina regeneration. *Cell Rep.* **9**, 272-284.
Zhu, M., Xin, T., Weng, S., Gao, Y., Zhang, Y., Li, Q. and Li, M. (2010). Activation of JNK signaling links lgl mutations to disruption of the cell polarity and epithelial organization in Drosophila imaginal discs. *Cell Res.* **20**, 242-245.

Supplementary experimental procedures

Temporal and spatial control of Eiger-expression

To induce expression of *eiger*, experiments were carried out as described in (Smith-Bolton et al., 2009) and in Fig.S1. Briefly, *rnGal4, UASegr, tubGal80^{TS}/TM6B, tubGal80* lines were outcrossed to a w^{1118} wild type strain or strains carrying indicated alleles or transgenes. Larvae were staged by collecting 50 1st instar larvae per vial 24 h after a 6 h egg collection. Larvae were raised at 18°C and shifted to 30°C for 40h at day 7 after egg deposition (D7 AED), unless noted otherwise. Genetic cell ablation experiments using *UASrpr; ptcGAL4, tubGAL80^{TS}* or *rnGal4, UASrpr, tubGal80^{TS}* were induced by a 16 h or a 24 h shift to 30°C at day 8 AED, respectively.

Flow cytometry

Flow cytometry analysis of wing imaginal disc cells was performed as described (de la Cruz and Edgar, 2008). Briefly, 20-30 dissected wing imaginal discs were dissociated in PBS with 9XTrypsin-EDTA (Sigma) supplemented with 1.5 µg/ml Hoechst 33342 for 2-3 h at room temperature. Cell profiles were obtained using a FACS Aria II instrument (BD Biosciences) and analysed using FlowJo 8.8.7 (Tree Star) software.

BrdU labelling

Larvae were dissected in Shields and Sang M3 medium and incubated for 30 min with 100µg/µl BrdU (Sigma) at room temperature. Cuticles were fixed in 4% PFA for 15 minutes and subsequently washed with 0.5% Triton X-100/PBS in all washing steps. Fixed tissues were incubated for 45 min in 2N HCl and washed with 0.1M H_3BO_3 for 2 min twice. Antibody incubations, sample mounting and analysis was carried out as described above.

Transcription factor binding site prediction

Bioinformatic analysis for potential transcription factor binding sites was performed using the program Clover (Cis-eLement OVERrepresentation) (Frith et al., 2004) in combination with position-weighted-matrices (PWM) obtained from the JASPAR collection (Mathelier et al., 2014). The p-value threshold of all predictions was set to $p<0.05$. *Drosophila* chromosome 2R was used as background sequence in all calculations. For each gene, genomic sequences (dm6 genome version) of 2.5 kb upstream from the transcriptional start site (TSS) and the entire first intron, if present, were selected for analysis. For short genes with a sequence shorter than 2 kb (e.g. *rpr* and *grim*) or for genes without introns, a 2.5 kb sequence downstream of the 3'UTR was add to the analysis. All results are documented in Supplemental .wig files. Data was visualized using USCS genome browser tools. mVISTA conservation analysis (Frazer et al., 2004, Bray et al., 2003) was run on *kay* and *hid* genomic

region by comparing *D.melanogaster* to: *D.simulans, D. sechellia, D. erecta, D. yakuba, D. ananassae, D. pseudobscura, D. persimilis, D. willistoni, D. virilis, D. grimshawi.* Genomic sequences were obtained from FlyBase. ATAC-seq profiles were previously published (Davie et al., 2015) (GEO access number: GSE59078) and used in this work as predictors of open chromatin regions.

Image analysis and quantification

General Information

Images were taken using 20X or 63X objectives (without additional optical zoom). Stacks were imaged at 1024x1024 pixel resolution and a z-step size of 1µm. Control and experimental samples were prepared under the same conditions on the same day, as well as imaged using the same conditions on the same day.

GFP volume quantification (G-trace lineage labelling)

Masks of the GFP signal were generated applying the 'Threshold' (settings: 'Triangle', stack histogram, dark background) and 'Remove Outliers' (settings: black and white pixels removal with radii= 1-10 at a constant threshold of 50) function to entire image stacks in FIJI. The resulting masks were analysed using the '3D Object Counter' function (settings: threshold= 128, min=10 max=Inf, Exclude Object On Edges=FALSE). Measured volumes for each disc were summed up and used to describe total GFP volume per disc.

pH3 and BrdU counts

Masks of pH3 (or BrdU) events per disc were generated by applying the 'Threshold' (settings: 'Li', stack histogram, dark background) and 'Remove Outliers' (settings: black and white pixels removal with radii= 1-5 at a constant threshold of 50) function to entire image stacks in FIJI. The resulting masks were analysed using the '3D Object Counter' function (settings: threshold= 128, min=10 max=Inf, Exclude Object On Edges=FALSE). The total number of counted particles was considered to represent mitotic or DNA replication events per disc.

pH3-positive mitotic events in G-trace lineage labelled cells (volumetric method)

To count the number of cells marked by pH3 within the GFP-positive, G-trace volume, the pH3 mask was 'Subtracted' (FIJI function) from the GFP mask. The resulting mask was analysed using the '3D Object Counter' function (settings: threshold= 128, min=10 max=Inf, Exclude Object On Edges=FALSE). The new total counts of particles were considered to be mitotic events in GFP-positive cells.

pH3-positive mitotic events in G-trace lineage labelled cells (absolute counts)

Nuclei of GFP-positive, cells were counted manually using the '*multi-point selection'* tool across stacks with z-step size of 2 µm. In the same disc, pH3-positive mitotic events within

the G-trace labelled region were manually counted across the entire stack. pH3 and nuclei counts were paired and ratios compared between genotypes.

TRE-reporter quantifications

Image stacks were manually curated to eliminate TRE-reporter activity signals arising from the peripodial membrane. The peripodium shows extensive TRE-reporter activity, which was not subject of this study. Maximum projections of the final image stacks were obtained in FIJI and

masks of the area with active reporter were generated using the 'Threshold' (settings: 'IsoData', stack histogram, dark background) and 'Remove Outliers' (settings: black and white pixels removal with radii=1-10 at a constant threshold of 50) function. The areas of resulting masks were quantified using the ROI analyzer in FIJI.

Supplementary Figures

Supplementary Figure 1. Experimental procedures

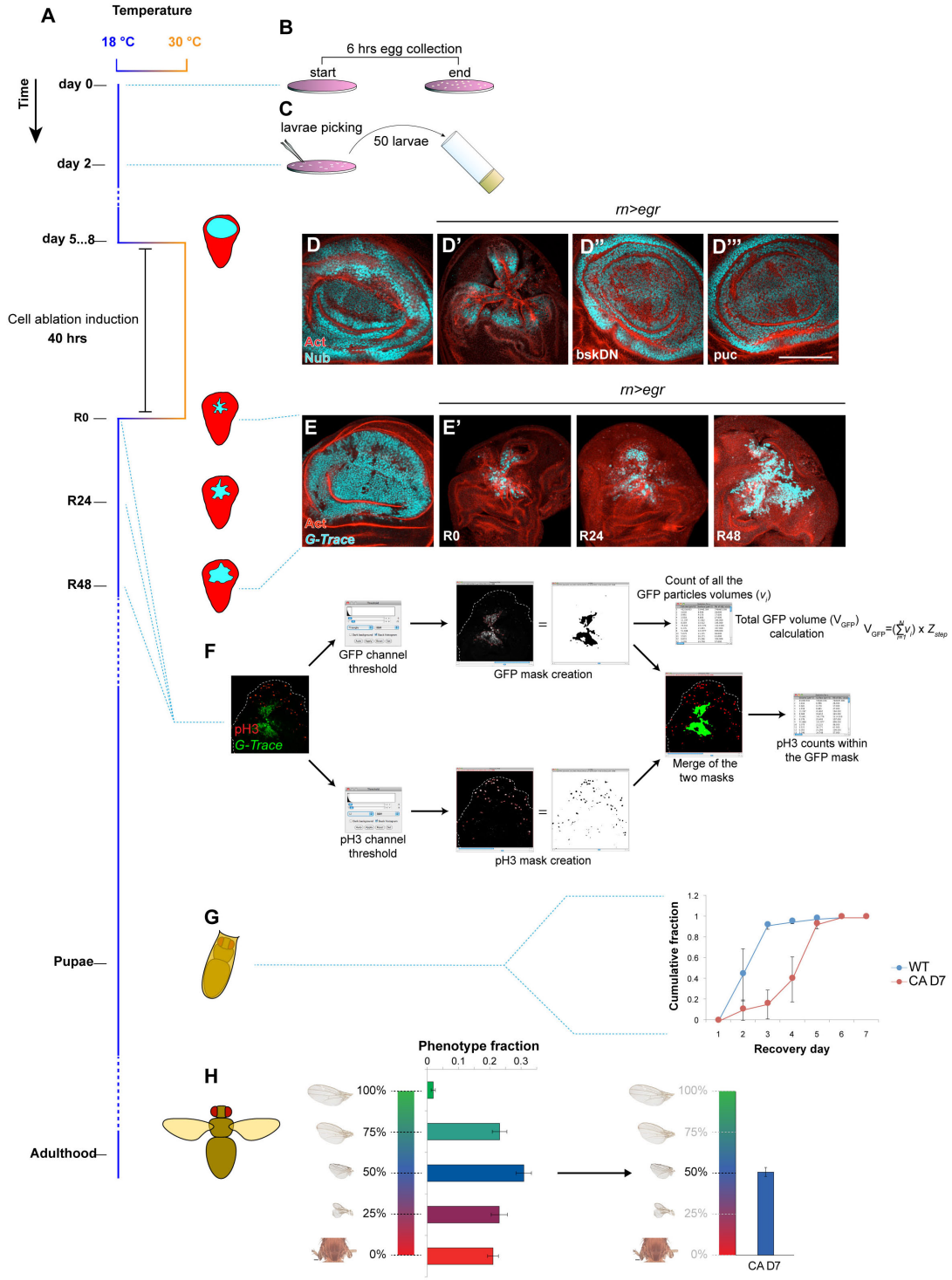

(A) Time line of development and induction of cell ablation by *eiger*-expression as a function of rearing temperature. Flies were raised at 18°C (blue) and transferred to 30°C (orange) for 40 hours to induce *eiger*-expression and cell ablation (CA) in wing imaginal discs. CA was

induced at different stages of development: 5 days (D5) after egg deposition (AED) or at day 6 (D6), day (D7) or day (D8). Unless otherwise noted, experiments were performed at D7.

(B) 6 hour egg collections were performed on grape juice plates (D0).

(C) 2 days after egg deposition (D2) 50 first instar larvae were collected in a vial.

(D) Wing pouch region in third instar wild type disc (D), wing disc after Eiger-mediated cell ablation at D7 (D'), wing disc after induction of *eiger*-expression with *rotund(rn)GAL4*-mediated co-expression a dominant-negative JNK (bskDN) (D'') or of the JNK-inhibitor Puckered (puc) (D''') stained for Actin (red) and for Nubbin (cyan) to visualize a lineage similar to *rnGAL4*-derived cells. Note that inhibition of JNK prevents Eiger-induced cell ablation.

(E) Wing pouch of a wild type disc, where cells of the *rnGAL4*-lineage were permanently labelled by GFP-expression using the GFP-lineage labelling system (*G-trace*). (E') *rnGAL4,* G-trace labelled cells which survived *eiger*-expression at recovery time point 0 hrs (R0), 24 hours (R24) and 48 hours (R48). Active proliferation of cells surviving *eiger*-expression contributes to compensatory proliferation.

(F) Schematic representation of automated workflows in Fiji to quantify volumes and particle counts in Eiger-stimulated discs.

(G) Cumulative fraction of larvae undergoing larval-pupal transitions, which carry wild type wing discs (WT) or wing discs that experienced *eiger*-expression for 40 h at D7 (CA). Compensatory responses to tissue stress induced by Eiger-mediated cell ablation induce a 2-day developmental delay at the larval to pupal transition.

(H) Quantification of average adult wing sizes developing from disc after Eiger-mediated cell ablation at D7. By scoring five different wing size phenotypes, quantifications were summarised as weighted averages of all different phenotypes (see Experimental procedures).

Supplementary Figure 2. Eiger-expression enables functional studies of JNK-dependent tissue stress responses

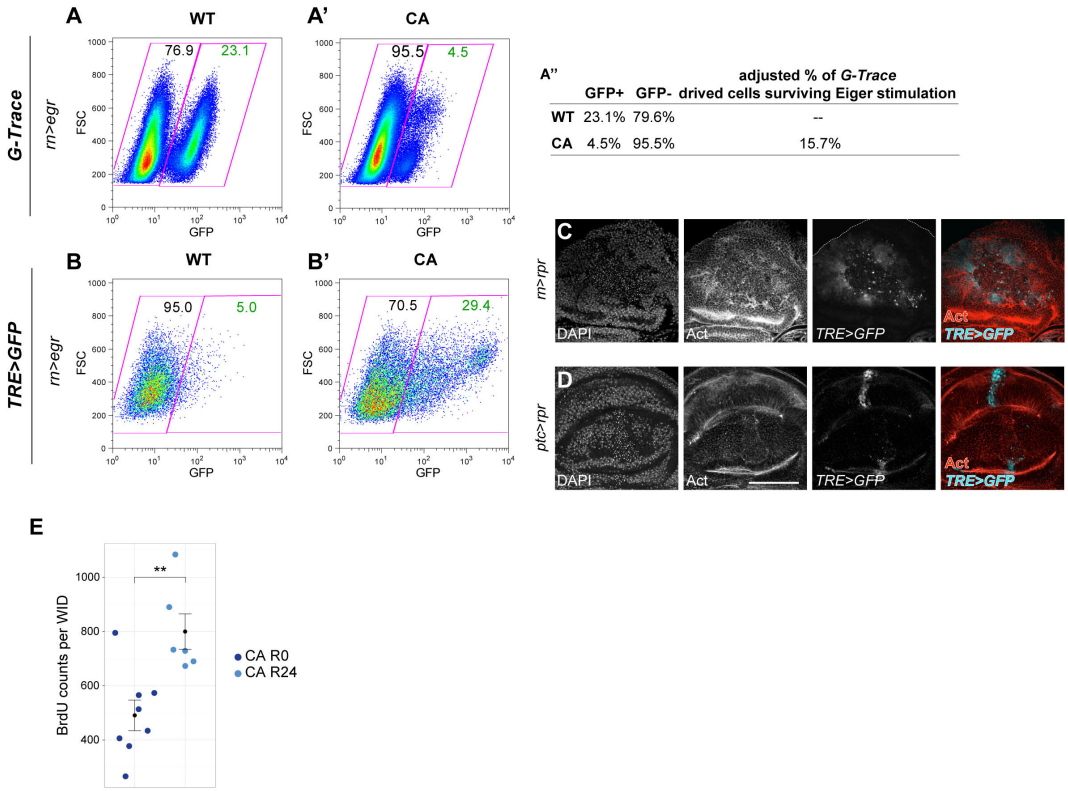

(A) FACS analysis of *rnGAL4,* G-trace-labelled cells expressing GFP in wild type **(A)** and in wing disc after Eiger-mediated cell ablation (A'). Data is plotted as a function of GFP-levels and forward scatter (FCS). To quantify the relative number of *rnGAL4,* G-trace-labelled cells that survive (A''), we made use of the following equation $X = (CA_{GFP+} * WT_{GFP-}) / (CA_{GFP-} * WT_{GFP+})$.

(B) FACS analysis of cells expressing the JNK reporter *TRE*-GFP in a wild type disc (B) and a wing disc after Eiger-mediated cell ablation (B'). Data is plotted as a function of GFP-levels and forward scatter (FCS).

(C, D) Wing pouch of discs expressing the JNK-reporter *TRE*-GFP (cyan in overlay), co-stained for DAPI or Actin (red in overlay). Discs were subjected to transient cell ablation driven by *rnGAL4, UAS-reaper* (rn>rpr) (C) or by *patched(ptc)GAL4, UAS-reaper* (ptc>rpr) (D). Compare to Fig.1B, C.

(E) Quantification of BrdU-positive events within Eiger-stimulated discs at R0 (n= 8 discs) and R24 (n= 6 discs).

Graphs display mean ± S.E.M. U-tests were performed to test for statistical significance (* *p<0.05, ** p<0.01, *** p<0.001*).

All scale bars: 100 µm.

Supplementary Figure 3. Eiger-induced tissue damage activates JAK/STAT signalling and tissue stress responses

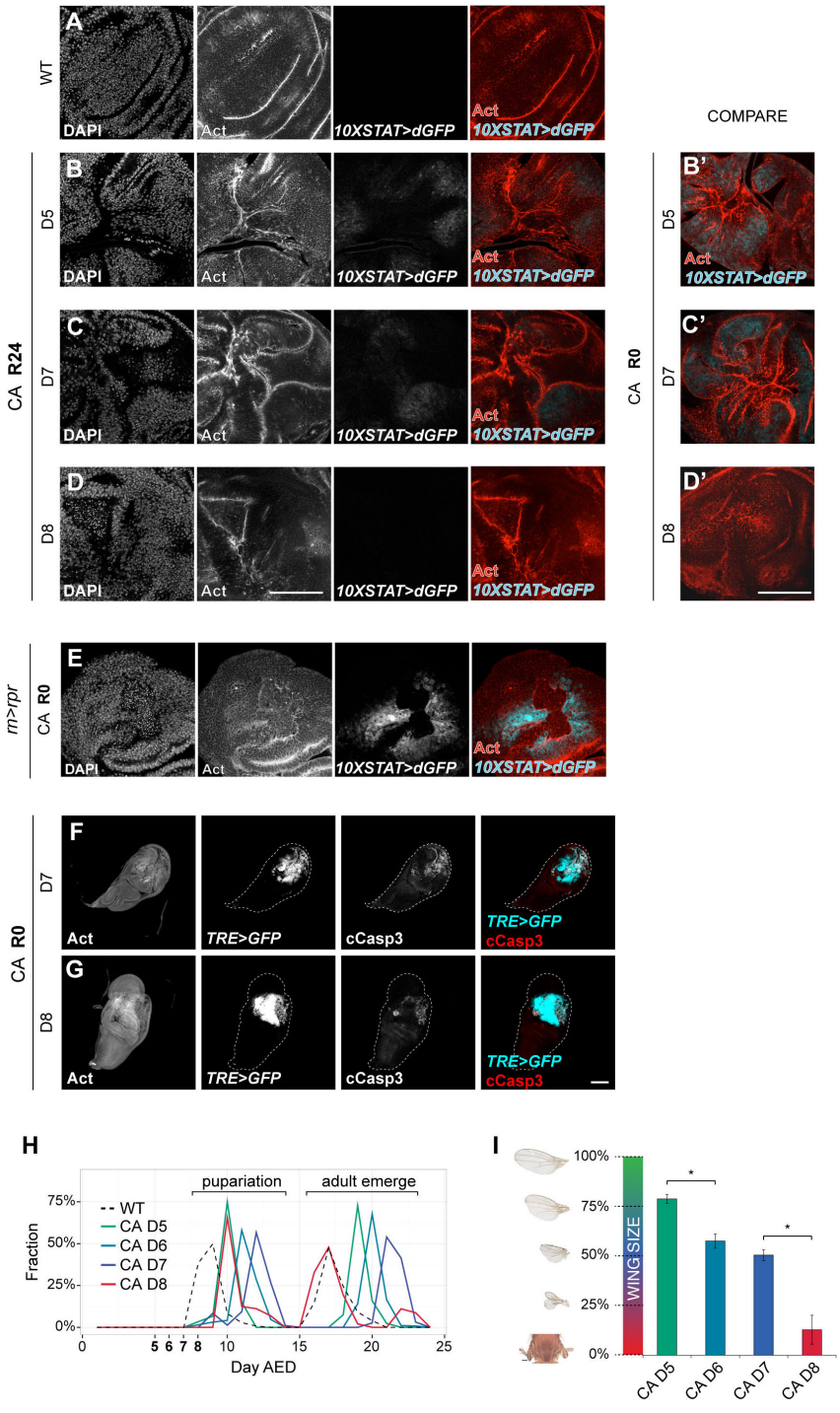

(A) Wing pouch in Eiger-stimulated discs (CA) expressing the JAK/STAT-reporter *10XSTAT*-dGFP (cyan in overlay), stained for DAPI or Actin (red in overlay).

(B-D) Wing pouch after *eiger*-expression was induced at developmental day 5 (B), day 7 (C) or day 8 (D) and imaged at R24. Discs express the JAK/STAT-reporter *10XSTAT*-dGFP (cyan

in overlay) and were stained for DAPI or Actin (red in overlay). Overlay images obtained at R0 are shown for comparison (B'-D').

(E) Wing pouch after transient cell ablation (CA) was induced by *rnGAL4, UAS-reaper* (rn>rpr). Disc expresses the JAK/STAT-reporter *10XSTAT*-dGFP (cyan in overlay), and was stained for DAPI and Actin (red in overlay). Compare to Fig. 2A.

(F, G) Wing discs after Eiger-stimulated cell ablation (CA) induced on D7 (F) or D8 (G). Discs expressing the JNK reporter *TRE*-GFP (cyan in overlay) were stained for Actin and for Cleaved Caspase-3 (cCasp3, red in overlay) to visualize apoptotic cells.

(H) Incident analysis of larva-to-pupal transition timing as well as adult eclosion timing in wild type animals and in animals where *eiger*-mediated CA was induced at D5, D6, D7 or D8.

(I) Quantification of average adult wing sizes developing from disc after *eiger*-mediated cell ablation was induced at D5, D6, D7 or D8.

All scale bars: 100 μm.

Supplementary Figure 4. JAK/STAT activation is not required for compensatory proliferation

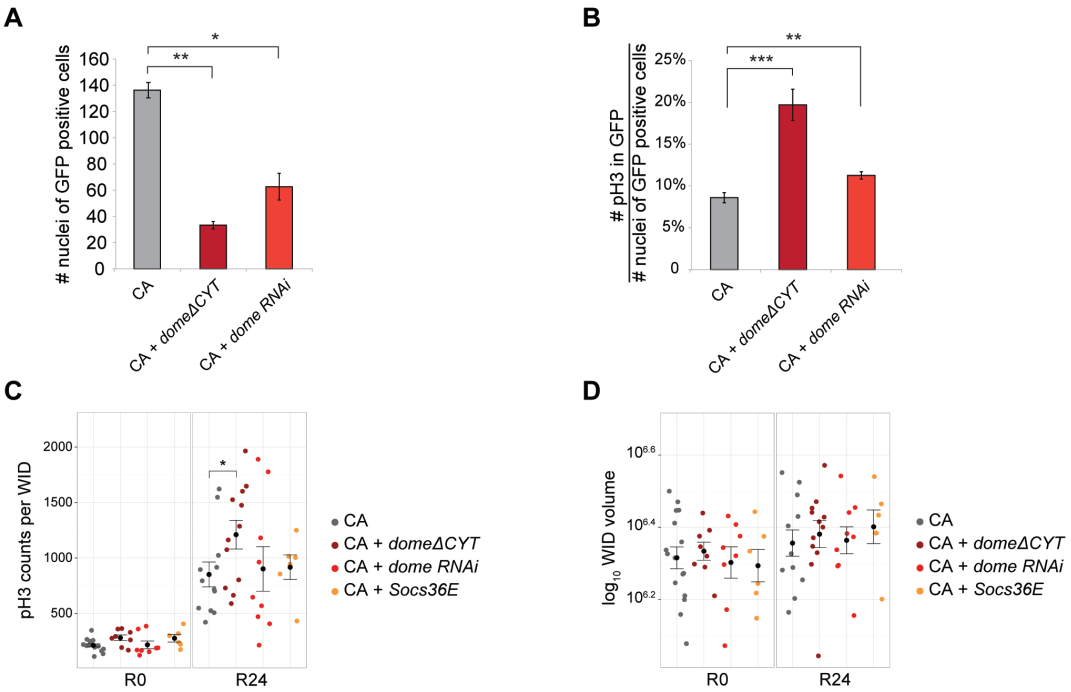

(A, B) Nuclear counts of G-trace labelled cells (B) and quantification of pH3-positive mitotic events within G-trace labelled cells (A) in ablated discs (CA) and ablated discs with *rnGAL4*-mediated co-expression of *dome*$^{\Delta cyt}$ or *dome* RNAi at R0 (for all samples n=3) in *eiger*-expressing cells.

(C, D) Quantification of pH3-positive, mitotic events per disc (A) and of total wing disc (WID) volume (B) at R0 and R24 after Eiger-stimulation. Wild type discs (CA) (R0 n=16, R24 n=12 discs) and discs with *rnGAL4*-mediated co-expression of *dome*$^{\Delta cyt}$ (R0 n= 8, R24 n=12 discs), *dome* RNAi (R0 n=8, R24 n= 9 discs) or *Socs36E* (R0 n= 6, R24 n= 6 discs) in *eiger*-expressing cells were quantified.

Graphs display mean ± S.E.M. U-test was run to check for statistical significance (* $p<0.05$; ** $p<0.01$; *** $p<0.001$).

Supplementary Figure 5. JAK/STAT activity is required for survival of Eiger-stimulated cells

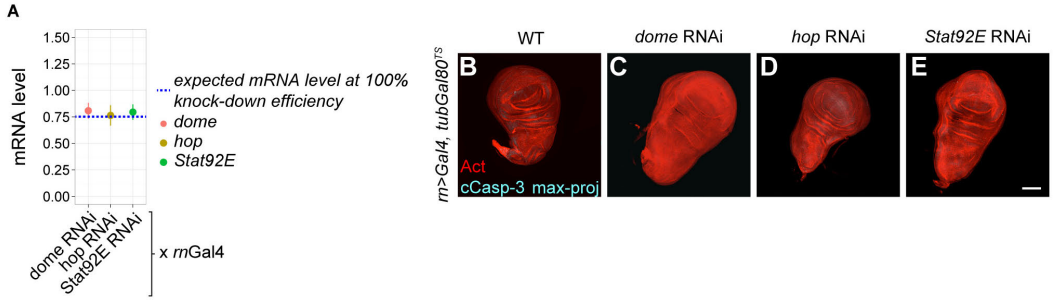

(A) Knock-down efficiency of UAS-RNAi transgenes targeting *dome, hop* and *Stat92E* was quantified by qRT-PCR. Wing imaginal discs expressing the constructs continuously under the control of *rnGAL4* were compared to wild type wing discs. Only about 25% of the total discs used for this analysis drives expression by *rnGAL4* (see Fig. S2A). Therefore the maximum expected reduction of transcript levels at 100% RNAi efficiency is only 25% (blue dashed line). Each graph shows mean ± S.E.M for n=2 biological replicates.

(B-E) Wild type wing disc (B) and wing discs with *rnGAL*4-driven expression of *dome* RNAi (C), *hop* RNAi (D) or *Stat92E* RNAi (E) induced at D7 for 40 hours were stained for Actin (red) and for Cleaved Caspase-3 (cyan) to visualize apoptotic cells. Maximum projections of entire image stacks are shown.

Graphs display mean ± S.E.M. U-tests were performed to test for statistical significance (* *p<0.05, ** p<0.01, *** p<0.001*).

All scale bars: 100 µm.

Supplementary Figure 6. A survival-promoting function of JAK/STAT is mediated by Zfh2

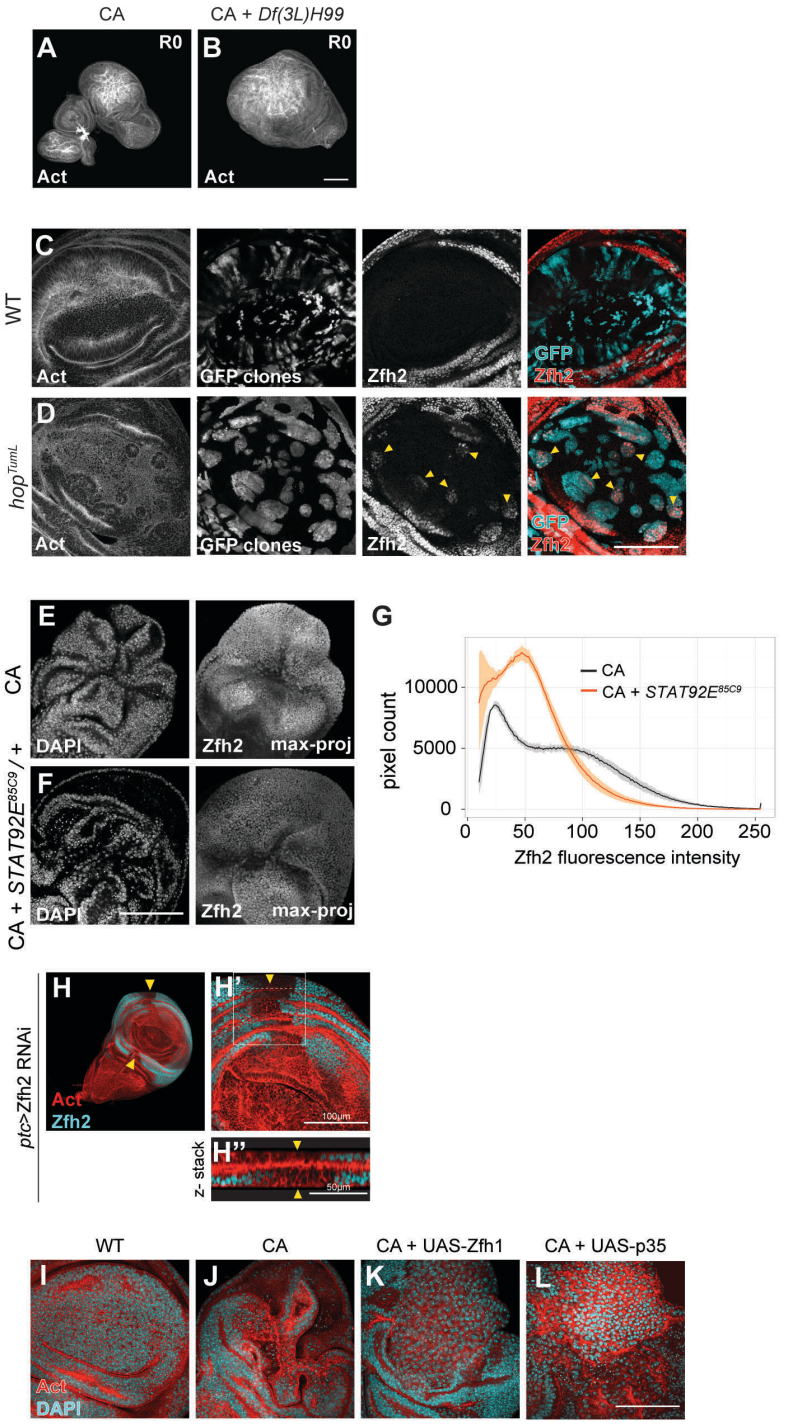

(A-B) Wild type wing disc (A) and wing disc heterozygous for *Df(3L)H99* (B) after Eiger-stimulated cell ablation were stained for Actin. Image in (A) also displays haltere and leg discs associated with the larger wing disc on the right.

(C-D) 'Flip-out' clones positively marked by expression of UAS-GFP under the control of Act5C-GAL4 (GFP clones, cyan in overlay) in wing discs stained for Zfh2 (red in overlay).

Clones were either wild type (C) or expressed a dominant active form of Hop (UAS-*hop*^{TumL}) (D). Yellow arrowheads indicate ectopic expression of Zfh2 in *Hop*^{TumL} expressing clones.
(E-F) Ablated discs (E) and ablated discs also heterozygous for *STAT92E*^{85c9} (F) were stained for DAPI and Zfh2. Maximum-projection images of the confocal stacks are shown.
(G) Pixel counts of Zfh2 fluorescence intensity quantified in stainings on ablated discs (gray line) and ablated discs also heterozygous for *STAT92E*^{85c9} (orange line). Each curve represents the average of n=3 independent measurements ± S.E.M.
(H) Wing disc expressing a RNAi construct targeting *zfh2* under the control of *ptcGAL4*. The disc was stained for Zfh2, confirming that Zfh2 signals disappeared in the *ptc* domain (yellow arrowheads, H, H'). Transverse section confirms loss of Zfh2 in the *ptc* domain (H'').
(I-L) Wild type wing disc (H), wing disc after Eiger-stimulation (I) and wing disc after Eiger-stimulation with *rnGAL4*-mediated co-expression of *Zfh1* (J) and *p35* (K) stained for DAPI (cyan) and Actin (red).
All scale bars: 100 μm unless otherwise noted.

Supplementary Figure 7. Prediction of AP-1 and ZFH binding sites on *hid* and *kay* loci.

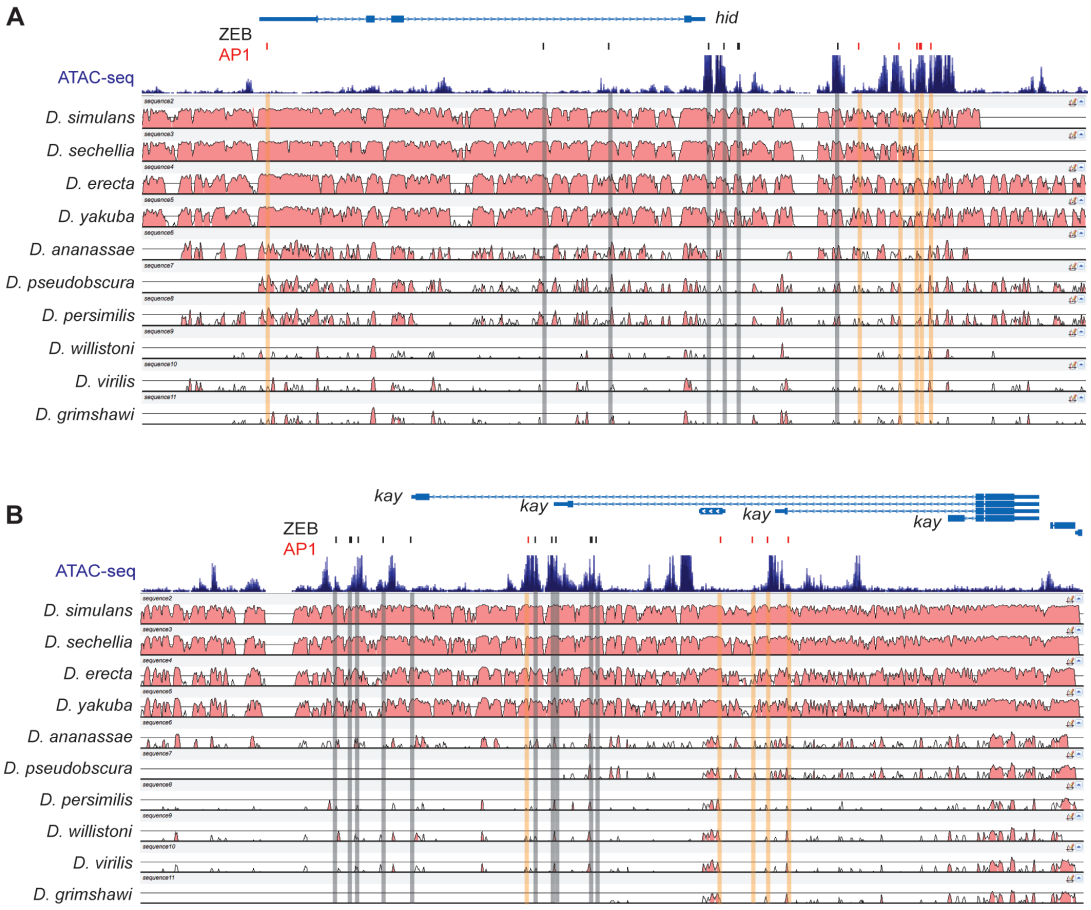

(A, B) Visualisation of AP-1 and ZEB/Zfh binding sites in regulatory regions of *hid* (A) *and fos (kay)* (B) predicted by bioinformatic analysis using Clover. ATAC-seq data (blue profile) from *D. mel.* wild type tissue, indicates open chromatin (Davie et al., 2015). mVISTA plots (red profiles) visualize conservation among *D. mel.* and species listed in the figure. Positions of predicted ZEB binding sites are shown in black/grey, predicted AP-1 binding sites in red/orange.

Supplementary Figure 8. JAK/STAT activity prevents excessive tissue damage in response to tissue stress

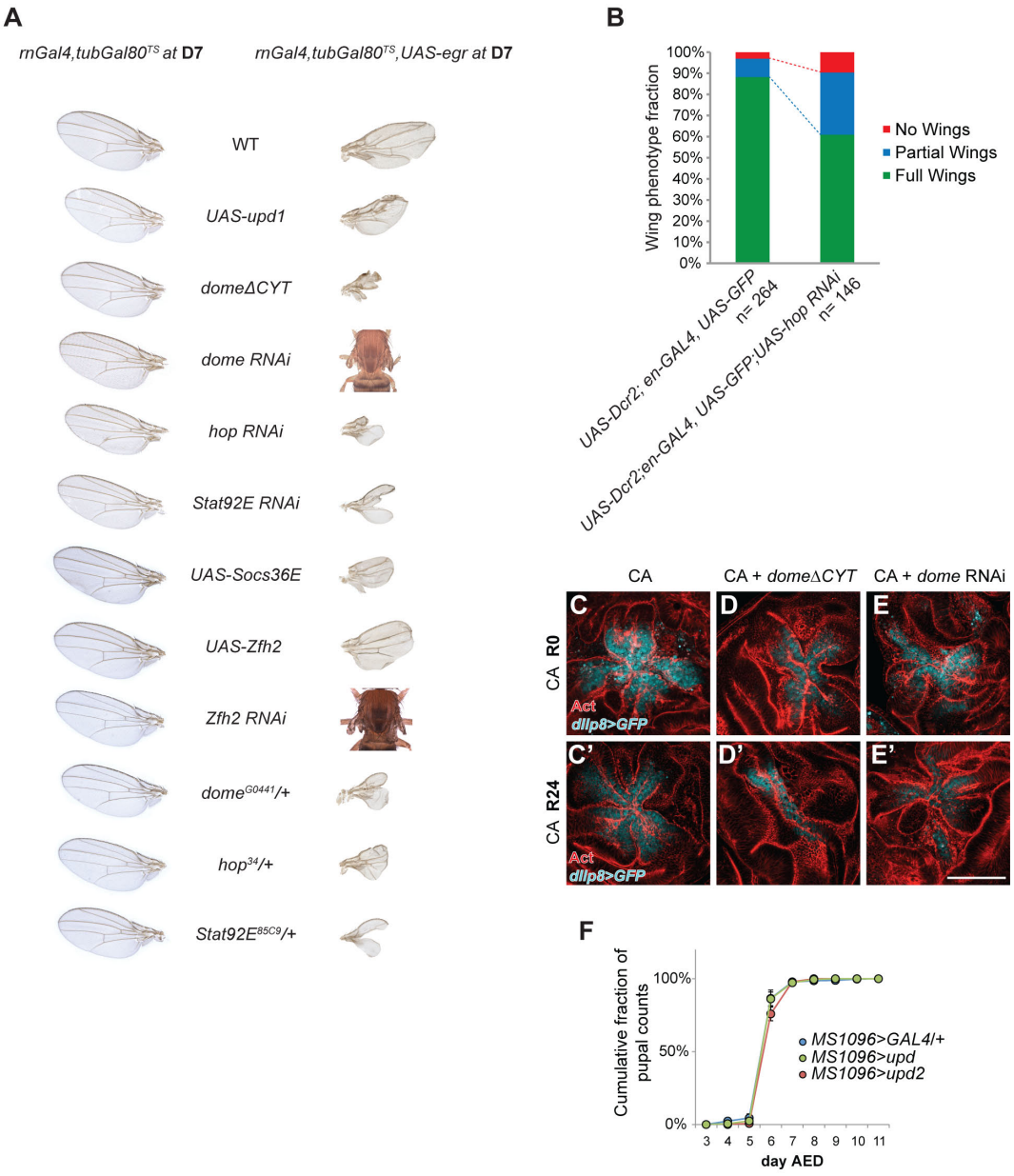

(A) Representative adult wings developing from wing discs having driven *rnGAL4*-mediated expression of UAS-transgenes at D7 or in genetic backgrounds heterozygous for *dome*^{G0441}, *hop*^{34}, or *Stat92E*^{85C9} alleles (left column). Representative adult wings developing from wing disc having driven *eiger*-expression and *rnGAL4*-mediated co-expression of UAS-transgenes at D7 or in genetic backgrounds heterozygous for *dome*^{G0441}, *hop*^{34}, or *Stat92E*^{85C9} alleles (right column).

(B) Quantification of 3 adult wing size classes developing from wing discs expressing GFP or GFP together with an RNAi-construct targeting *hop* in the posterior compartment. All wing discs were injured during larval development by targeted pinching using forceps.
(C-E) Wing disc after after Eiger-mediated cell ablation (CA) (C) and discs combined with *rnGAL4*-mediated co-expression of $dome^{\Delta cyt}$ (B) or *dome* RNAi (C) in *eiger*-expressing cells, imaged at R0 (C-D) and R24 (C'-E') expressing the *dILP8*-GFP reporter (cyan) and stained for Actin (red).
(F) Cumulative fraction of larvae undergoing larval-pupal transitions, which carry control discs (MS1096GAL4/+) and discs expressing *upd* or *upd2* under the control of *MS1096*GAL4. Graph shows mean ± S.D. for average scores from at least 3 independent experiments.

Supplementary Figure 9. Models of how a survival-promoting function of JAK/STAT contributes to restoration of tissue homeostasis

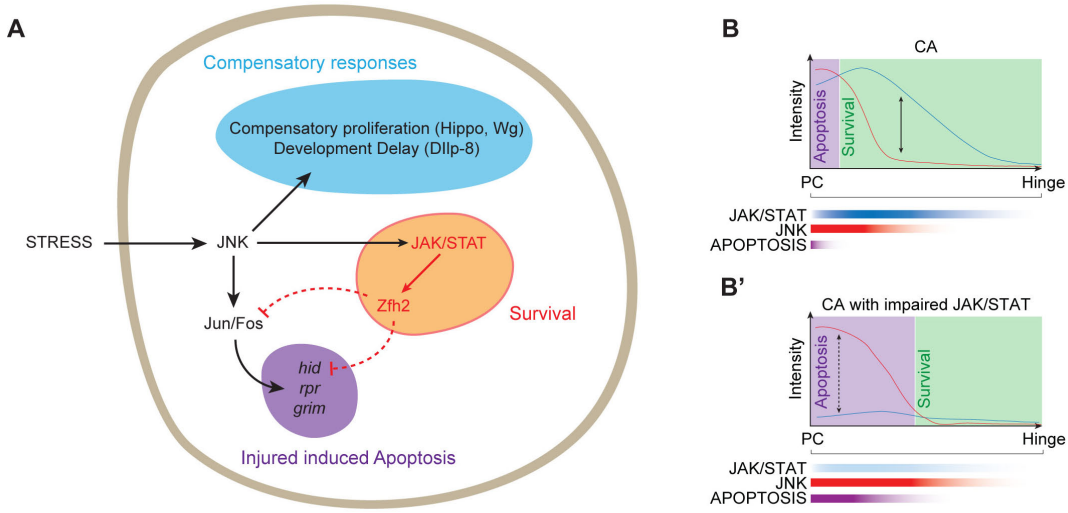

(A) Cells that activate JNK signalling in response to tissue stress induce compensatory responses as well as injured-induced apoptosis. JAK/STAT activates Zfh-2 to repress *hid* and *fos (kay),* thereby limiting strong JNK-activation and Hid-induced apoptosis. Suppression of apoptosis limits the extent of tissue damage and promotes compensatory responses by cells surviving JNK activation. This facilitates activation of compensatory proliferation and induction of development delays.

(B) Non-autonomous activation of JNK and of JAK/STAT creates two differently sloped signalling gradients from the site of damage (cell ablation (CA) in the pouch centre (PC)). A low JNK/JAKSTAT ratio induces apoptosis, whereas a high low JNK/JAKSTAT ratio promotes survival.

(B') If the JAK/STAT signalling gradient is disturbed (f.e. by heterozygosity for JAK/STAT components) all cells with JNK signalling have a low JNK/JAKSTAT ratio, making them more likely to die. Higher levels of apoptosis near the site of damage (PC) induce stronger non-autonomous activation of JNK, which in turn induces apoptosis at sites more distant to the initial damage. This feed-forward loop, unrestrained by loss of JAK/STAT activity, drives spatial expansion of JNK signalling and apoptosis, thereby increasing the extent of tissue damage and limiting the ability of the tissue to induce regenerative responses.

References

BRAY, N., DUBCHAK, I. & PACHTER, L. 2003. AVID: A global alignment program. *Genome Res,* 13**,** 97-102.

DAVIE, K., JACOBS, J., ATKINS, M., POTIER, D., CHRISTIAENS, V., HALDER, G. & AERTS, S. 2015. Discovery of Transcription Factors and Regulatory Regions Driving In Vivo Tumor Development by ATAC-seq and FAIRE-seq Open Chromatin Profiling. *PLoS Genet,* 11**,** e1004994.

DE LA CRUZ, A. F. & EDGAR, B. A. 2008. Flow cytometric analysis of Drosophila cells. *Methods Mol Biol,* 420**,** 373-89.

FRAZER, K. A., PACHTER, L., POLIAKOV, A., RUBIN, E. M. & DUBCHAK, I. 2004. VISTA: computational tools for comparative genomics. *Nucleic Acids Res,* 32**,** W273-9.

FRITH, M. C., FU, Y., YU, L., CHEN, J. F., HANSEN, U. & WENG, Z. 2004. Detection of functional DNA motifs via statistical over-representation. *Nucleic Acids Res,* 32**,** 1372-81.

MATHELIER, A., ZHAO, X., ZHANG, A. W., PARCY, F., WORSLEY-HUNT, R., ARENILLAS, D. J., BUCHMAN, S., CHEN, C. Y., CHOU, A., IENASESCU, H., LIM, J., SHYR, C., TAN, G., ZHOU, M., LENHARD, B., SANDELIN, A. & WASSERMAN, W. W. 2014. JASPAR 2014: an extensively expanded and updated open-access database of transcription factor binding profiles. *Nucleic Acids Res,* 42**,** D142-7.

SMITH-BOLTON, R. K., WORLEY, M. I., KANDA, H. & HARIHARAN, I. K. 2009. Regenerative growth in Drosophila imaginal discs is regulated by Wingless and Myc. *Dev Cell,* 16**,** 797-809.

Table S1. Genotypes and experimental conditions. This table lists all fly lines, their sources and the derived genotypes used to generate the data for each of the main and supplementary figures in this study. Experimental conditions related to induction of Eiger-expression are listed to the right.

General information	Genotypes	Source
	w^{1118}	
	rn-Gal4,UAS-egr,tub-GAL80^{TS}/TM6b, tub-GAL80^{TS}	I Hariharan, R Smith-Bolton
	UAS-FLP,Ubi-p63E.FRT>STOP>FRT-Stinger15F2	Bloomington
	TRE-RFP	D Bohmann
	TRE-GFP	D Bohmann
	UAS-Bsk^{DN}	Bloomington
	UAS-puc	Bloomington
	10XSTATdGFP/Cyo	E Bach
	dome^{G0441}/FM7, ubi-GFP	Bloomington
	hop^{34}/FM7, ubi-GFP	N Perrimon
	FRT82-Stat92E^{85C9}/TM6c	E Bach
	UAS-dome$^{\Delta CYT}$/Cyo, ubi-GFP	E Bach
	UAS-Socs36E	E Bach
	zfh2[EAB]	F. J. Díaz-Benjumea and E. Sánche
	UAS-upd1/Cyo, ubi-GFP	M Zeidler
	w; UAS-upd2/Cyo	M Zeidler
	dilp8-GFP	Bloomington
	w; FRT 82B	Bloomington
	yw, ey-FLP; act>y^{+}>GAL4, UAS-GFP/Cyo;FRT82B, tub-GAL80/TM6b	G Halder
	yw, ey-FLP; UAS-Ras^{V12}/Cyo,FRT82B, scrib^{2}/TM6b	G Halder
	UAS-Ras^{V12}/Cyo; FRT82B, scrib^{2}, Stat92E^{85C9}/Tm6b	G Halder
	UAS-p35	Bloomington
	UAS-domeRNAi /Cyo, ubi-GFP	VDRC-KK106071
	UAS-hopRNAi	BL-HMS00761
	UAS-hopRNAi	BL-JF01268
	UAS-Stat92ERNAi	BL-HMS00035
	UAS-zfh1.P	Bloomington
	UAS-zfh1RNAi/TM3, Sb	BL-JF02509
	UAS-zfh2RNAi/TM6b	VDRC-GD13305
	Df(3L)H99/TM3, Sb	Bloomington
	UAS-Dcr2/FM7i;en-Gal4,UAS-GFP	Bloomington
	MS1096-Gal4/FM7a;Sp/Cyo;Dr/TM6c	
	ex[e1]-lacZ/SM6	G Halder
	upd-LacZ/FM7a	
	UAS-Hop^{TumL}/CyO	N Perrimon
	STAT92E-GFP.FLAG/CyO;Dr/TM6c	Bloomington
	hsflp[122]/+; act>y[+]>GAL4,UAS-GFP/+	

Figures	Genotypes	raised at	temperature shift	AED
Figure 1				
1A	*+/+;rn-Gal4,tub-Gal80^{TS}/UAS-FLP,Ubi-p63E-FRT>STOP>FRT-Stinger15F2*	18°C	30°C, 40 h	7d
1A',1D,1F	*+/+;rn-Gal4,UAS-egr,tub-Gal80^{TS}/UAS-FLP,Ubi-p63E-FRT>STOP>FRT-Stinger15F2*	18°C	30°C, 40 h	7d
1B	*TRE-GFP/+;+/+*	18°C	30°C, 40 h	7d
1C	*TRE-RFP/+;rn-Gal4,UAS-egr,tub-Gal80^{TS}/UAS-FLP,Ubi-p63E-FRT>STOP>FRT-Stinger15F2*	18°C	30°C, 40 h	7d
1E,1G	*+/+;rn-Gal4,UAS-egr,tub-Gal80^{TS}/+*	18°C	30°C, 40 h	7d
Figure 2				
2A	*10XSTATdGFP/+;+/+*	18°C	30°C, 40 h	5d-7d-8d
2B-D	*10XSTATdGFP/+;rn-Gal4,UAS-egr,tub-Gal80^{TS}/+*	18°C	30°C, 40 h	5d-7d-8d
2E	*+/+;rn-Gal4,UAS-egr,tub-Gal80^{TS}/+*	18°C	30°C, 40 h	5d-7d-8d
Figure 3				
3A,3E-F	*+/+;rn-Gal4,UAS-egr,tub-Gal80^{TS}/+*	18°C	30°C, 40 h	7d
3B,3E-3F	*dome^{G0441}/+;+/+;rn-Gal4,UAS-egr,tub-Gal80^{TS}/+*	18°C	30°C, 40 h	7d + 6h
3C,3E-3F	*hop^{34}/+;+/+;rn-Gal4,UAS-egr,tub-Gal80^{TS}/+*	18°C	30°C, 40 h	7d + 6h
3D,3E-3F	*+/+;rn-Gal4,UAS-egr,tub-Gal80^{TS}/FRT82-Stat92E^{85C9}*	18°C	30°C, 40 h	7d + 12h

3G,3K-3L	*+/+;rn-Gal4,UAS-egr,tub-Gal80^{TS}/UAS-FLP,Ubi-p63E-FRT>STOP>FRT-Stinger15F2*	18°C	30°C, 40 h	7d
3H,3K-3L	*UAS-domeΔCYT/+;rn-Gal4,UAS-egr,tub-Gal80^{TS}/UAS-FLP,Ubi-p63E-FRT>STOP>FRT-Stinger15F2*	18°C	30°C, 40 h	7d
3I,3K-3L	*UAS-domeRNAi/+;rn-Gal4,UAS-egr,tub-Gal80TS/UAS-FLP,Ubi-p63E-FRT>STOP>FRT-Stinger15F2*	18°C	30°C, 40 h	7d
3J,3K-3L	*UAS-Socs36E/+;rn-Gal4,UAS-egr,tub-Gal80TS/UAS-FLP,Ubi-p63E-FRT>STOP>FRT-Stinger15F2*	18°C	30°C, 40 h	7d
Figure 4				
4A,4E,4I	*+/+;rn-Gal4,UAS-egr,tub-Gal80^{TS}/+*	18°C	30°C, 40 h	7d
4B,4E	*UAS-domeΔCYT/+;rn-Gal4,UAS-egr,tub-Gal80^{TS}/+*	18°C	30°C, 40 h	7d
4C,4E	*UAS-domeRNAi/+;rn-Gal4,UAS-egr,tub-Gal80TS/+*	18°C	30°C, 40 h	7d
4D-E	*+/+;rn-Gal4,UAS-egr,tub-Gal80TS/UAS-Socs36E*	18°C	30°C, 40 h	7d
4F,4I	*dome^{G0441}/+;+/+;rn-Gal4,UAS-egr,tub-Gal80^{TS}/+*	18°C	30°C, 40 h	7d + 6h
4G,4I	*hop^{34}/+;+/+;rn-Gal4,UAS-egr,tub-Gal80^{TS}/+*	18°C	30°C, 40 h	7d + 6h
4H-I	*+/+;rn-Gal4,UAS-egr,tub-Gal80^{TS}/FRT82-Stat92E^{85C9}*	18°C	30°C, 40 h	7d + 12h
4J,4N	*TRE-RFP/+;rn-Gal4,UAS-egr,tub-Gal80^{TS}/+*	18°C	30°C, 40 h	7d
4K,4N	*dome^{G0441}/+;TRE-RFP/+;rn-Gal4,UAS-egr,tub-Gal80^{TS}/+*	18°C	30°C, 40 h	7d + 6h
4L,4N	*hop^{34}/+;TRE-RFP/+;rn-Gal4,UAS-egr,tub-Gal80^{TS}/+*	18°C	30°C, 40 h	7d + 6h
4M-N	*TRE-RFP/+;rn-Gal4,UAS-egr,tub-Gal80^{TS}/FRT82-Stat92E^{85C9}*	18°C	30°C, 40 h	7d + 12h
Figure 5				
5A, 5C, 5E, 5G	*w118*			
5A-M	*+/+;rn-Gal4,UAS-egr,tub-Gal80^{TS}/+*	18°C	30°C, 40 h	7d
5B	*+/+;rn-Gal4,UAS-egr,tub-Gal80^{TS}/FRT82-Stat92E^{85C9}*	18°C	30°C, 40 h	7d
5I	*+/+;rn-Gal4,UAS-egr,tub-Gal80TS/UAS-Zfh2RNAi*	18°C	30°C, 40 h	7d
5K	*+/+;rn-Gal4,UAS-egr,tub-Gal80^{TS}/UAS-FLP,Ubi-p63E-FRT>STOP>FRT-Stinger15F2*	18°C	30°C, 40 h	7d
5L	*+/+;rn-Gal4,UAS-egr,tub-Gal80^{TS}/+;Zfh2[EAB]*	18°C	30°C, 40 h	7d
Figure 6				
6A-D	*+/+;rn-Gal4,UAS-egr,tub-Gal80^{TS}/+*	18°C	30°C, 40 h	7d
6B-C	*UAS-upd1/+;+/+;rn-Gal4,UAS-egr,tub-Gal80^{TS}/+*	18°C	30°C, 40 h	7d
6B	*UAS-upd2/+;+/+;rn-Gal4,UAS-egr,tub-Gal80^{TS}/+*	18°C	30°C, 40 h	7d
6B-C	*UAS-domeΔCYT/+;rn-Gal4,UAS-egr,tub-Gal80^{TS}/+*	18°C	30°C, 40 h	7d
6B-C	*UAS-domeRNAi/+;rn-Gal4,UAS-egr,tub-Gal80TS/+*	18°C	30°C, 40 h	7d
6B-C	*+/+;rn-Gal4,UAS-egr,tub-Gal80TS/UAS-hopRNAi*	18°C	30°C, 40 h	7d
6B	*+/+;rn-Gal4,UAS-egr,tub-Gal80TS/UAS-STAT92ERNAi*	18°C	30°C, 40 h	7d
6B	*+/+;rn-Gal4,UAS-egr,tub-Gal80TS/UAS-Socs36E*	18°C	30°C, 40 h	7d
6B	*+/+;rn-Gal4,UAS-egr,tub-Gal80TS/UAS-Zfh2RNAi*	18°C	30°C, 40 h	7d
6B	*+/+;rn-Gal4,UAS-egr,tub-Gal80^{TS}/+;Zfh2[EAB]*	18°C	30°C, 40 h	7d
6B	*dome^{G0441}/+;+/+;rn-Gal4,UAS-egr,tub-Gal80^{TS}/+*	18°C	30°C, 40 h	7d + 6h
6B	*hop^{34}/+;+/+;rn-Gal4,UAS-egr,tub-Gal80^{TS}/+*	18°C	30°C, 40 h	7d + 6h
6B	*+/+;rn-Gal4,UAS-egr,tub-Gal80^{TS}/FRT82-Stat92E^{85C9}*	18°C	30°C, 40 h	7d + 12h
6D	*+/+;rn-Gal4,UAS-egr,tub-Gal80^{TS}/dllp8-GFP*	18°C	30°C, 40 h	7d
6D	*UAS-domeΔCYT/+;rn-Gal4,UAS-egr,tub-Gal80^{TS}/dllp8-GFP*	18°C	30°C, 40 h	7d
6D	*UAS-domeRNAi/+;rn-Gal4,UAS-egr,tub-Gal80TS/dllp8-GFP*	18°C	30°C, 40 h	7d
Figure 7				
7A,7D-E,7F,7I,7J,7M	*yw,ey-FLP;act>y+>GAL4,UAS-GFP/+;FRT82B,tub-GAL80/FRT82B-iso*	25°C		
7B,7D-E,7G,7I,7K,7M	*yw,ey-FLP;act>y+>GAL4,UAS-GFP/UAS-Ras^{V12};FRT82B, tub-GAL80/FRT82B,scrib^{2}*	25°C		
7C-E,7H-I,7L-M	*yw,ey-FLP;act>y+>GAL4,UAS-GFP/UAS-Ras^{V12};FRT82B, tub-GAL80/FRT82B,scrib^{2},Stat92E^{85C9}*	25°C		

Supplementary figures

Figures	Genotypes	raised at	exp. conditions	
Figure S1				
S1D,S1G	*w118*	18°C	30°C, 40 h	7d
S1D',S1G-H	*+/+;rn-Gal4,UAS-egr,tub-Gal80^{TS}/+*	18°C	30°C, 40 h	7d
S1D"	*UAS-bskDN/+;+/+;rn-Gal4,UAS-egr,tub-Gal80^{TS}/+*	18°C	30°C, 40 h	7d
S1D"'	*+/+;rn-Gal4,UAS-egr,tub-Gal80^{TS}/UAS-puc*	18°C	30°C, 40 h	7d
S1E	*+/+;rn-Gal4,tub-Gal80^{TS}/UAS-FLP,Ubi-p63E-FRT>STOP>FRT-Stinger15F2*	18°C	30°C, 40 h	7d
S1E'-F	*+/+;rn-Gal4,UAS-egr,tub-Gal80^{TS}/UAS-FLP,Ubi-p63E-FRT>STOP>FRT-Stinger15F2*	18°C	30°C, 40 h	7d

Figure S2				
S2A	*+/+;rn-Gal4,tub-Gal80^{TS}/UAS-FLP,Ubi-p63E-FRT>STOP>FRT-Stinger15F2*	18°C	30°C, 40 h	7d
S2A'	*+/+;rn-Gal4,UAS-egr,tub-Gal80^{TS}/UAS-FLP,Ubi-p63E-FRT>STOP>FRT-Stinger15F2*	18°C	30°C, 40 h	7d
S2B	*TRE-GFP/+;+/+*	18°C	30°C, 40 h	7d
S2B'	*TRE-GFP/+;rn-Gal4,UAS-egr,tub-Gal80^{TS}/+*	18°C	30°C, 40 h	7d
S2C	*TRE-GFP/+;rn-Gal4,UAS-rpr,tub-Gal80^{TS}/+*	18°C	30°C, 24 h	7d
S2D	*UAS-rpr/+;ptc-Gal4,tub-Gal80^{TS}/TRE-GFP;+/+*	18°C	30°C, 16 h	7d
S2E	*+/+;rn-Gal4,UAS-egr,tub-Gal80^{TS}/+*	18°C	30°C, 40 h	7d
Figure S3				
S3A	*10XSTATdGFP/+;+/+*	18°C	30°C, 40 h	7d
S3B-D	*10XSTATdGFP/+;rn-Gal4,UAS-egr,tub-Gal80^{TS}/+*	18°C	30°C, 40 h	5d-7d-8d
S3E	*10XSTATdGFP/+;rn-Gal4,UAS-rpr,tub-Gal80^{TS}/+*	18°C	30°C, 24 h	7d
S3F-G	*TRE-GFP/+;rn-Gal4,UAS-egr,tub-Gal80^{TS}/+*	18°C	30°C, 40 h	7d-8d
S3H-I	*+/+;rn-Gal4,UAS-egr,tub-Gal80^{TS}/+*	18°C	30°C, 40 h	5d-6d-7d-8d
Figure S4				
S4A-D	*+/+;rn-Gal4,UAS-egr,tub-Gal80^{TS}/+*	18°C	30°C, 40 h	7d
S4A-D	*UAS-domeΔCYT/+;rn-Gal4,UAS-egr,tub-Gal80^{TS}/+*	18°C	30°C, 40 h	7d
S4A-D	*UAS-domeRNAi/+;rn-Gal4,UAS-egr,tub-Gal80TS/+*	18°C	30°C, 40 h	7d
S4C-D	*UAS-Socs36E/+;rn-Gal4,UAS-egr,tub-Gal80TS/+*	18°C	30°C, 40 h	7d
Figure S5				
S5A	*+/+;rn-Gal4/+*	21°C		
S5A	*UAS-domeRNAi/+;rn-Gal4/+*	21°C		
S5A	*+/+;rn-Gal4/UAS-hopRNAi*	21°C		
S5A	*+/+;rn-Gal4/UAS-STAT92ERNAi*	21°C		
S5B	*+/+;rn-Gal4,tub-Gal80^{TS}/+*	18°C	30°C, 40 h	7d
S5B	*UAS-domeRNAi/+;rn-Gal4,tub-Gal80TS/+*	18°C	30°C, 40 h	7d
S5B	*+/+;rn-Gal4,tub-Gal80TS/UAS-hopRNAi*	18°C	30°C, 40 h	7d
S5B	*+/+;rn-Gal4,tub-Gal80TS/UAS-STAT92ERNAi*	18°C	30°C, 40 h	7d
Figure S6				
S6A,S6E, S6J	*+/+;rn-Gal4,UAS-egr,tub-Gal80^{TS}/+*	18°C	30°C, 40 h	7d
S6B	*+/+;rn-Gal4,UAS-egr,tub-Gal80^{TS}/Df(3L)H99*	18°C	30°C, 40 h	7d
S6C	*hsflp [122]/+;+/+, ubi-GFP; act>y[+]>GAL4,UAS-GFP/+*	21°C	37°C, 15 min	
S6D	*hsflp [122]/+;UAS-Hop^{TumL}/+; act>y[+]>GAL4,UAS-GFP/+*	21°C	37°C, 15 min	
S6H-H"	*ptc-Gal4,tub-Gal80TS/+;UAS-Zfh2RNAi/+*	18°C	30°C, 40 h	7d
S6F	*+/+;rn-Gal4,UAS-egr,tub-Gal80^{TS}/FRT82-Stat92E^{85C9}*	18°C	30°C, 40 h	7d
S6I	*w118*	18°C	30°C, 40 h	7d
S6K	*UAS-Zfh1/+;rn-Gal4,UAS-egr,tub-Gal80^{TS}/+*	18°C	30°C, 40 h	7d
S6L	*UAS-p35/+;rn-Gal4,UAS-egr,tub-Gal80^{TS}/+*	18°C	30°C, 40 h	7d
Figure S7				
S7A	*+/+;rn-Gal4,UAS-egr,tub-Gal80^{TS}/+*	18°C	30°C, 40 h	7d
S7A	*UAS-upd1/+;+/+;rn-Gal4,UAS-egr,tub-Gal80^{TS}/+*	18°C	30°C, 40 h	7d
S7A	*UAS-upd2/+;+/+;rn-Gal4,UAS-egr,tub-Gal80^{TS}/+*	18°C	30°C, 40 h	7d
S7A	*UAS-domeΔCYT/+;rn-Gal4,UAS-egr,tub-Gal80^{TS}/+*	18°C	30°C, 40 h	7d
S7A	*UAS-domeRNAi/+;rn-Gal4,UAS-egr,tub-Gal80TS/+*	18°C	30°C, 40 h	7d
S7A	*+/+;rn-Gal4,UAS-egr,tub-Gal80TS/UAS-hopRNAi*	18°C	30°C, 40 h	7d
S7A	*+/+;rn-Gal4,UAS-egr,tub-Gal80TS/UAS-STAT92ERNAi*	18°C	30°C, 40 h	7d
S7A	*+/+;rn-Gal4,UAS-egr,tub-Gal80TS/UAS-Socs36E*	18°C	30°C, 40 h	7d
S7A	*+/+;rn-Gal4,UAS-egr,tub-Gal80TS/UAS-Zfh2RNAi*	18°C	30°C, 40 h	7d
S7A	*+/+;rn-Gal4,UAS-egr,tub-Gal80^{TS}/+;Zfh2[EAB]*	18°C	30°C, 40 h	7d
S7A	*dome^{G0441}/+;+/+;rn-Gal4,UAS-egr,tub-Gal80^{TS}/+*	18°C	30°C, 40 h	7d + 6h
S7A	*hop^{34}/+;+/+;rn-Gal4,UAS-egr,tub-Gal80^{TS}/+*	18°C	30°C, 40 h	7d + 6h
S7A	*+/+;rn-Gal4,UAS-egr,tub-Gal80^{TS}/FRT82-Stat92E^{85C9}*	18°C	30°C, 40 h	7d + 12h
S7A	*+/+;rn-Gal4,tub-Gal80^{TS}/+*	18°C	30°C, 40 h	7d
S7A	*UAS-upd1/+;+/+;rn-Gal4,tub-Gal80^{TS}/+*	18°C	30°C, 40 h	7d

S7A	*UAS-upd2/+;+/+;rn-Gal4,tub-Gal80^{TS}/+*	18°C	30°C, 40 h	7d
S7A	*UAS-domeΔCYT/+;rn-Gal4,tub-Gal80^{TS}/+*	18°C	30°C, 40 h	7d
S7A	*UAS-domeRNAi/+;rn-Gal4,tub-Gal80TS/+*	18°C	30°C, 40 h	7d
S7A	*+/+;rn-Gal4,tub-Gal80TS/UAS-hopRNAi*	18°C	30°C, 40 h	7d
S7A	*+/+;rn-Gal4,tub-Gal80TS/UAS-STAT92ERNAi*	18°C	30°C, 40 h	7d
S7A	*+/+;rn-Gal4,tub-Gal80TS/UAS-Socs36E*	18°C	30°C, 40 h	7d
S7A	*+/+;rn-Gal4,tub-Gal80TS/UAS-Zfh2RNAi*	18°C	30°C, 40 h	7d
S7A	*+/+;rn-Gal4,tub-Gal80^{TS}/+;Zfh2[EAB]*	18°C	30°C, 40 h	7d
S7A	*dome^{G0441}/+;+/+;rn-Gal4,tub-Gal80^{TS}/+*	18°C	30°C, 40 h	7d + 6h
S7A	*hop^{34}/+;+/+;rn-Gal4,tub-Gal80^{TS}/+*	18°C	30°C, 40 h	7d + 6h
S7A	*+/+;rn-Gal4,tub-Gal80^{TS}/FRT82-Stat92E^{85C9}*	18°C	30°C, 40 h	7d + 12h
S7B	*UAS-dcr2/+;en-Gal4,UAS-GFP/+;+/+*	25°C		
S7B	*UAS-dcr2/+;en-Gal4,UAS-GFP/+;UAS-hopRNAi/+*	25°C		
S7C	*+/+;rn-Gal4,UAS-egr,tub-Gal80^{TS}/dIlp8-GFP*	18°C	30°C, 40 h	7d
S7D	*UAS-domeΔCYT/+;rn-Gal4,UAS-egr,tub-Gal80^{TS}/dIlp8-GFP*	18°C	30°C, 40 h	7d
S7E	*UAS-domeRNAi/+;rn-Gal4,UAS-egr,tub-Gal80TS/dIlp8-GFP*	18°C	30°C, 40 h	7d
S7F	*MS1096-Gal4/+;+/+;+/+*	25°C		
S7F	*MS1096-Gal4/UAS-upd1;+/+;+/+*	25°C		
S7F	*MS1096-Gal4/UAS-upd2;+/+;+/+*	25°C		

Table S2. Primers used for real--time qPCR analysis.

Gene		Seq.	5' - 3'
	upd1	Fwr	TCGATATGCGCTTTGTGAAG
	upd1	Rev	TGCTGCTGCTGTAGCAACTT
	upd2	Fwr	TACAAGTTCCTGCCGAACATGAC
	upd2	Rev	ACAAGTGGCGATTCTATAAGGGAAAC
	upd3	Fwr	CCCCTGAAGCACCTACAGAA
	upd3	Rev	AGGATCCTTTGGCGTTTCTT
	dome	Fwr	ATCGCAAAGAATACAAAATAAATTACAAAC
	dome	Rev	TCTGGAATCTGGAAACTAGAAACCAC
	hop	Fwr	TATCCGGATTTGGTATGGATGAATG
	hop	Rev	TTTTTAAAACAACACAAGCCAGACC
	STAT92E	Fwr	CATGCAATGTGCTCTTCACA
	STAT92E	Rev	AGATCTGGACGTGCTTTGCT
	hid	Fwr	ACAACTTCTTCCGGCAGCAG
	hid	Rev	GAAGGGAGGGGAATGGTGTG
	rpr	Fwr	CGACTCTGTTGCGGGAGG
	rpr	Rev	GGCTTGCGATATTTGCCGGA
	grim	Fwr	GTCGGAGTTTGGATGCTGGG
	girm	Rev	AGTCACGTCGTCCTCATCGT
	zfh1	Fwr	ACGAGCAGAGCAACATGAGC
	zfh1	Rev	CGGCGACATTTTGTTAGCAC
	zfh2	Fwr	TGCACACACAACAGATGCGT
	zfh2	Rev	GCACAGCTGACAAAGGAGCA
	kay	Fwr	CGAATAGCAAGAATCAGCTGGAGTA
	kay	Rev	CTGTCGTTGCTGTTGTGGTTGT
Housekeeping	*Act5C*	Fwr	GGCGCAGAGCAAGCGTGGTA
Housekeeping	*Act5C*	Rev	GGGTGCCACACGCAGCTCAT
Housekeeping	*αTub84B*	Fwr	TGGGCCCGTCTGGACCACAA
Housekeeping	*αTub84B*	Rev	TCGCCGTCACCGGAGTCCAT
Housekeeping	*RpL32*	Fwr	AAGCGGCGACGCACTCTGTT
Housekeeping	*RpL32*	Rev	GCCCAGCATACAGGCCCAAG
Housekeeping	*RpL13A*	Fwr	AGCTGAACCTCTCGGGACAC
Housekeeping	*RpL13A*	Rev	TGCCTCGGACTGCCTTGTAG